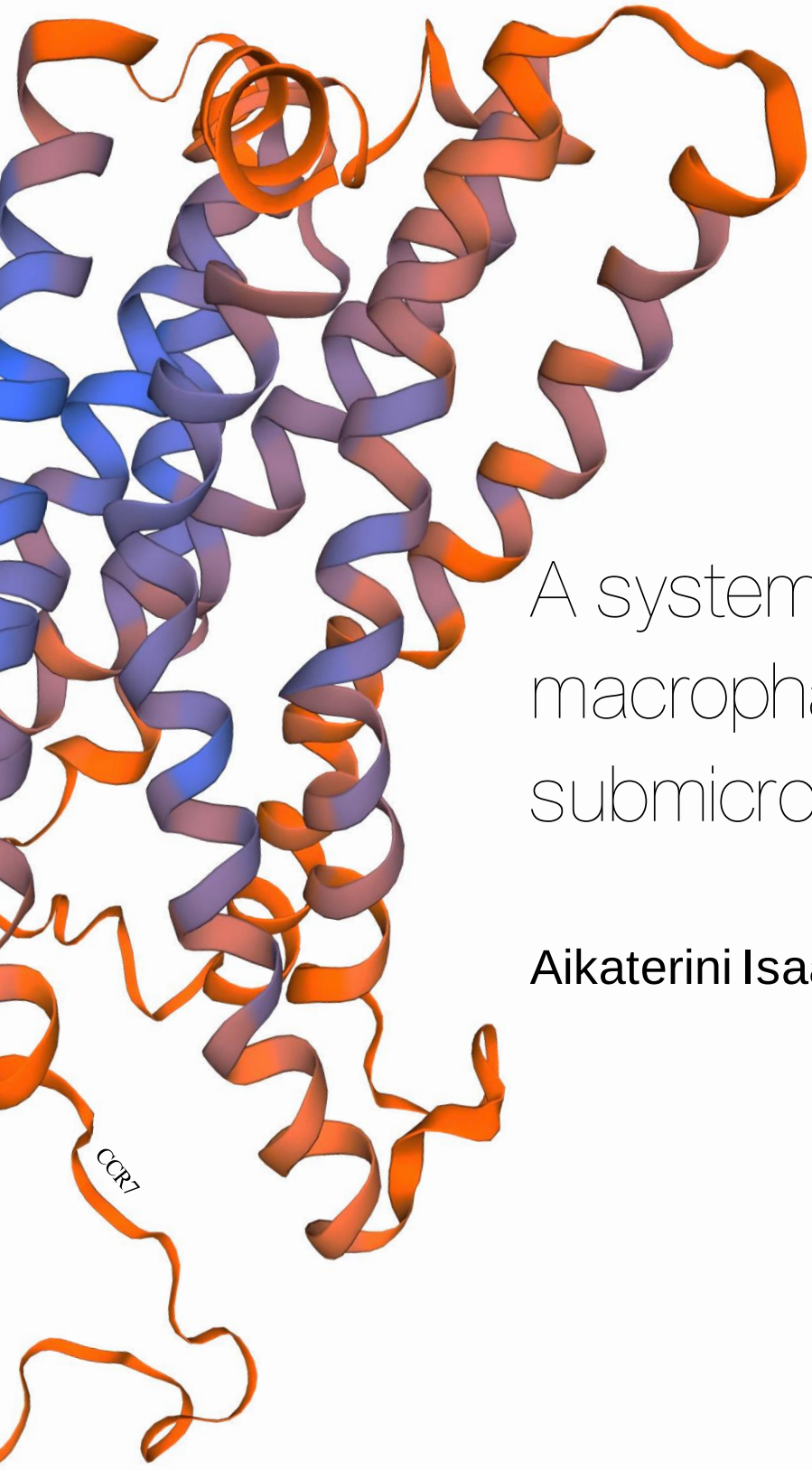

A systematic study of macrophages' response to submicron pillars

Aikaterini Isaakidou

TU Delft

Page intentionally left blank

A systematic study of macrophages' response to submicron pillars.

A systematic study of the effect of submicron pillar topographies on the murine cell line J774A.1

By

Aikaterini Isaakidou
4738225

in partial fulfilment of the requirements for the degree of

Master of Science
in Biomedical Engineering

at the Delft University of Technology,
to be defended publicly on December 12, 2019

Supervisors: Prof. dr. Amir A. Zadpoor, TU Delft
Assistant prof. dr. ir. E.L. Fratila-Apachitei, TU Delft
PhD candidate Mahdiyeh Nouri Goushki, TU Delft

Thesis Committee: Prof. dr. Amir A. Zadpoor, TU Delft
Assistant prof. dr. ir. E.L. Fratila-Apachitei, TU Delft
Assistant prof. dr. E.C.M. Carroll, TU Delft
PhD candidate Mahdiyeh Nouri Goushki, TU Delft

This thesis is confidential and cannot be made public until December 12, 2021

An electronic version of this thesis is available at http://repository.tudelft.nl/.

TU Delft

Page intentionally left blank

Preface

This thesis is the last step towards completing a journey that began about two years ago. The choice of this route has its own story, but for now that is irrelevant. It all started in September 2017, when I arrived in Delft to begin the master programme of Biomedical Engineering and found myself impressed and overwhelmed with awe after each lecture. In June of 2018, after completing the so-called difficult part of the master programme, collecting these coveted 60 ECTS from courses, I realized that I could do it again. I could attend the same and more lecture hours and being stunned by the grandeur of the human body. The plethora of the existing but also yet undisclosed knowledge on human physiology as well as my desire to be actively involved, led me at the office door of my supervisor, professor E.L Fratila-Apachitei, who I had to persuade of my motivation, since my technical background was not very well suited to the team's research. Finally, she trusted me, and I thank her for the opportunity she gave me to start exploring an amazing scientific field. All of the above may sound palaver words of an overly ambitious and arrogant person to the reader. To that very skeptical reader, I would like to say that in the following pages he/she will find a description of an experimental process that was performed and documented with complete respect to the human and material resources that were available and is dedicated to all those who will spend some of their time to listen to a beautiful story.

Thank you very much.

"Once upon a time, there was a not-so-little girl, living in a south-east province of the Netherlands, in the city of Delft, who decided to study the potential of some topographies in modulating the response of a very crucial cell type in the human body, the macrophages. Did she succeed on that? We will find out in the following pages…."

Aikaterini Isaakidou

Page intentionally left blank

If you have any notion of where you are going, you will never get anywhere.
-Joan Miro, In Search of Genius

Page intentionally left blank

Contents

Abbreviations

2PP	Two-photon polymerization
ARG-1	Arginase I
BMP	Bone morphogenetics protein
BSA	Bovine serum albumin
Calcein AM	Calcein acetoxymethyl
CCR7 or CD197	C-C chemokine receptor type 7
CD206	Mannose receptor
DAPI	4′,6-diamidino-2-phenylindole
DMEM	Dulbecco's Modified Eagle's medium
DWL	Direct Writing Laser
EBL	Electron beam lithography
ERK	Extracellular-signal-regulated kinase
Eth-1	Ethidium homodimer 1
FBGCs	Foreign Body Giant Cells
FIBL	Focused ion beam lithography
IF	Immunofluorescence
IL-4,	Family of interleukins
INF-γ	Interferon gamma
IPA	2-Propanol
LIL	Laser interference lithography
LPS	Lipopolysaccharide
MAPK	Mitogen-activated protein kinase
NIL	Nanoimprint lithography
NOS	Nitric oxide synthases
NOS-1	Nitric oxide synthase 1 (neuronal)
NOS-2 or iNOS	Nitric oxide synthase 2 (inducible isoform)
NOS-3 or eNOS	Nitric oxide synthase 3 (endothelial)
PBS	Phosphate-buffered saline
PFA	Paraformaldehyde
PGMEA	Propanediol monomethyl ether acetate
PMNs	Polymorphonuclear leukocytes
ROS	Reactive oxygen species
SEM	Scanning electron microscopy
TNF-α	Tumor necrosis factor alpha

Page intentionally left blank

Abstract

Objective: Advances in the field of biomaterials have positively affected implant acceptance and nowadays, nanostructured surfaces are known to have possible beneficial effects on bone regeneration. The development of the field of osteoimmunology has contributed to a steadily increasing interest towards the investigation of the immunomodulatory effect of nanopatterned surfaces. Luckily, advances in nanofabrication methods have resulted in fabricating relatively large nanostructured areas with high resolution. This study is taking advantage of the 3D printing technique called two-photon polymerization (2PP) for the generation of submicron pillar arrays (patterns) to systematically investigate their effect on murine macrophages regarding cell viability, attachment, morphology and phenotype polarization.

Methods: Patterns with 3 different heights (300 nm, 500 nm and 1000 nm) and 2 different pitches (700 nm and 1000 nm) were fabricated. The pillars were characterized by using scanning electron microscopy (SEM). Viability of J774A.1 macrophages on the patterns was assessed by live/dead staining with calcein AM and ethidium homodimer-1. Cell attachment to the patterns and cell morphology were studied using SEM imaging. The phenotype polarization of the macrophages on the patterns was explored by dual immunofluorescent staining of M1/M2 markers.

Results: The different pillar heights and pillar pitches induced different cell attachment mechanisms and directly affected cell morphology after one day of seeding. The patterns with a height of 1000 nm and a pitch of 700 nm caused an increase in the number of elongated cells. The rounded cells showed larger areas on the patterns with a pitch of 1000 nm. Elongated macrophages were strongly affected by the patterns with 1000 nm height and 700 nm pitch. Moreover, patterns with a pillar height and pitch of 1000 nm exhibited the M1 to M2 phenotype switch.

Keywords: Biomaterials, osteoimmunology, nanofabrication, topographies, macrophages, M1, M2, cytoskeleton, phenotype

Page intentionally left blank

Acknowledgements

I would like to thank my professor dr. ir. E. Lidy Fratila-Apachitei for giving me the opportunity to get involved in such an interesting project and the guidance and support she has provided me with through each stage of my graduation project.
I would also like to thank Mahdiyeh Nouri Goushki and PhD candidate at the department, for being my daily supervisor.
Special thanks to Michelle Minneboo, supervisor of my biological work at the Cytocompatibility Lab of the Department, for her constant encouragement, the insightful discussions we had during my thesis and her prompt help with imaging for the last part of my thesis.
To Khashayer Modaresifar, PhD candidate at the department, for his assistance during the last weeks and to Daniel Fan for introducing me to the Nanoscribe system and for being there to answer questions as well as cheering up the dull cleanroom environment.
Last but not least, thanks to all the colleagues and fellows that I met, talked and worked with. Thanks to Angeliki Dimaraki and Sebastian Callens, lab colleagues, for all the laughs and the complaining sessions we shared. To Ahmed Sharaf, Nanoscribe user, with whom we spent the whole summer working on our prints at Nanoscribe and share difficulties and successes. To Christos Christoforidis, fellow master student, for the daily routine we shared all these months. Sincere thanks to all my friends for these amazing 2 years and the loving times with you. Wish you success and personal happiness.
Last but not least, deep-hearted thanks to my parents, Konstantinos and Smaragda, and my brothers, Periklis and Lefteris, for their unconditional love, support and belief in me.

Page intentionally left blank

1 Introduction

Implants and prosthetics are medical devices used to restore function and promote healing after injuries or diseases. Their presence dates to antiquity, when in ancient Egypt wood was used to restore amputated limps [1]. Findings of the renaissance period show that prosthetics have been fabricated by iron during this period. Along the centuries, the materials used for implants have become very sophisticated and complex. Materials like wood and iron were gradually replaced by metal alloys, polymers, composites and in the 21st century they can even be a combination of synthetic and natural materials. These materials, nowadays called biomaterials, can be classified according to their origin, chemical composition, mechanical properties, shape, dimensions, interaction with the host, biodegradability, duration of contact, application type and application site.

The growth of the field of biomaterials is reflected in the market growth. The continuous ageing of the population across the globe results in an upward trend of the market values for biomaterials. An increasing incidence of musculoskeletal diseases, traumas and osteoarthritis has a leading effect on the development of the orthopedics market growth. According to economic forecasts, the total market value in the orthopedics worldwide is estimated to reach a value of US$ 58.4 million with an annual growth of 3.55% until 2027 [2].

Integration of the implant in the host is one very decisive factor for implant's success. In this direction, surgical procedures and aseptic techniques have been improved to achieve implant acceptance. Although early acceptance is mostly successful, there is a big percentage of implant failures taking place even 7.5 years after implantation, as demonstrated by studies on total hip replacement surgeries [3]. Implant failures require revision surgeries, that are more susceptible to failure and increase the health risks for the patients, as they require longer hospitalization period and higher antibiotics dosage to prevent infection. For the aforementioned reasons, the new generation of orthopedic implants are designed and manufactured with special properties that promote bone growth around the implant ensuring a direct and effective coupling of the bone with the implant. This process is known as osseointegration. Implant acceptance is also inextricably linked with the biocompatibility of the implant material. Biocompatibility is the ability of the material from which the implant is made, to serve its purpose and initiate the intended host response for the specific application. An absolutely biocompatible material would theoretically provoke no inflammation, nor a chronic host response, however this is not realizable. Instead of that, the evolution of the research is tending towards a synergetic relationship between the host and the biomaterial. In this direction, the field of biomaterials has benefited from advances in life sciences and engineering lately and more specifically, it is now easier than it ever was to fabricate very complex structures even at nanoscale sizes with high resolution and incorporate proteins or hydrogels to mimic the natural tissue properties for *in vitro* and *in vivo* experiments.

Understanding the events that occur right after the placement of an implant in the host give a nice overview of the properties that biomaterials should possess. The cascade of these events starts when blood proteins and proteins from the interstitial fluids come in contact with the implant and adhere on its surface forming a matrix on the implant surface. Subsequently, this matrix formation activates coagulation leading to blood clot formation also initiating the acute inflammation phase. During this phase, neutrophils (PMNs) and mast cells arrive at the implant site. Neutrophils arrive first and their enzymatic activity aims at implant surface degradation while mast cells undergo degranulation excreting compounds that enhance the inflammatory response. As a result, monocytes are recruited to the site and differentiate into macrophages. They can digest particles of up to approximately 3 μm and if the particle is of a greater size,

they form clusters of cells, called Foreign Body Giant Cells (FBGCs) to phagocytize them. At this point, the implantation site, the biomaterial type as well as the tissue type contribute to the success or failure of the implant. One of the most common adverse effects, for example, is implant encapsulation. The FBGCs will attract fibroblasts to the site, that will deposit a collagenous film on the implant surface resulting in implant isolation from the host and loss of function. On the other hand, the initial inflammatory response can result in the initiation of osteoinduction and new bone formation, followed by bone remodelling. A visual representation of this process is given in Figure 1.

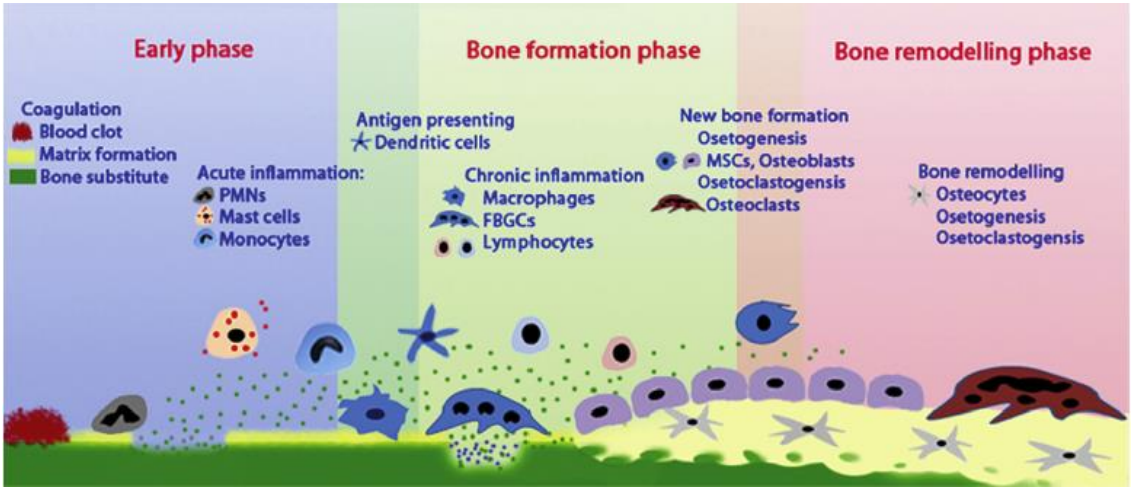

Figure 1: Bone formation phases [4]

The numbers of the early inflammatory cell types vary along the inflammatory process. The initial high number in neutrophils is declining as monocytes take over. This happens because neutrophils have a lifetime of up to 48 hours, whereas monocyte emigration to the implantation site lasts for weeks and monocytes can differentiate to macrophages that can live up to months [5]. Macrophages are versatile blood cells that contribute to tissue development and tissue repair while also defending the organism against pathogens, inflammation, fibrosis and cancer. The pivotal role of macrophages regarding bone healing has become evident as they have been lately related with bone morphogenetics protein (BMP) expression that contributes to bone formation [6]. The diversity, presence and necessity of macrophages in all tissue types has given rise to an increasing interest on the biomolecular mechanisms that induce various macrophage behaviors. Moreover, the development of osteoimmunology, the cross-disciplinary field that explores the interactions of the skeleton system with the immune system, has provided a stronger ground to investigate macrophages' responses related to bone growth.

Macrophages are classified as classically, and alternatively activated macrophages and they are identified as M1 and M2 macrophages respectively. The M1 macrophage phenotype is antigen-presenting and is expressed in the presence of pro-inflammatory substances like INF-γ and LPS and produce pro-inflammatory cytokines of the interleukin family (IL-1β, IL-6, IL-12, IL-23), TNF-α, and high levels of reactive oxygen species (ROS) activity. The M2 macrophage phenotype is expressed in the presence of IL-4, IL-13 and IL-10, they produce IL-10 and they also present receptors for specific glycoproteins like mannose and galactose. The trade-off between the M1/M2 population and activity is believed to play a crucial role in bone healing events. Prolong expression of the M1 phenotype is said to be detrimental for implant acceptance and would lead to chronic inflammation and fibrous encapsulation of the implant while a timely switch to the M2 phenotype could lead to osseointegration of the implant. Apart from those chemical cues that can affect M1/M2 macrophage polarization, physical cues are reportedly considered to have an effect. Cells react to nanoscale structures, by reason of the

collagen nanofibrils that are present in the extracellular matrix (ECM) and also because their receptors (filopodia, lamellipodia etc.) are nanostructures [7]. The process by which extracellular mechanical forces are causing intracellular biochemical changes are within the sphere of the mechanism known as mechanotransduction. There are two different mechanisms for cell signaling transduction proposed, the direct and the indirect mechanotransduction. In the direct mechanotransduction mechanism, the structural components of the cytoskeleton (microfilaments, microtubules, intermediate filaments) are transferring the mechanical forces exerted on the cytoskeleton to the nucleus, resulting in changes in the cell morphology and biochemical behaviour, by chromosome rearrangement [8]. The activation of the extracellular-signal-regulated kinase (ERK)/mitogen-activated protein kinase (MAPK) pathway is the key factor enabling indirect mechanotransduction. The pathway consists of a series of proteins that convey a signal from the receptor on the surface of the cell to the nucleus with consequent DNA changes. It has been implied that these two mechanisms are interwoven, since ligand (ERK/MAPK) and mechanical signaling take place conjunctionally [9].

Implant surfaces are very rarely flat as it is more likely that they possess a surface structure depending on the fabrication technique. The surface topography of implants can be divided in 3 categories; the micro-scale topographies (>1 μm), the submicron topographies (100 nm-1000 nm) and the nanoscale topographies (< 100nm). A lot of research has been performed on developing techniques that can precisely fabricate topographies on biomaterials along the years. The topographies found in the literature can be classified based on their level of organization to rough topographies and patterns. Rough topographies are characterized by a high level of randomness and lack of a specific minimal feature morphology, whereas patterns consist of one specific repetitive minimal feature morphology. In multiple studies, the effect of a variety topographies on macrophages has been investigating, most of the times combined with osteogenic and osteoimmunomodulatory properties. For example, tubules not only affect macrophage polarization but also show a good osteogenic profile in the range of d=78-170nm, p =18-30nm and h=700nm-1000nm. Porous structures of 200 nm constrain bone resorption and at the same time pores of 50-100 nm activate bone-formation pathways. Studies on pillars showed that diameters in the range between 200-300nm can induce positive osteogenic effects [10-14]. Randomly oriented fibers in microscale sizes yielded worst results than aligned submicron scale fibers of approximately 500 nm diameter at both *in vivo* and *in vitro* studies [15-17]. Grooves in general induced an inflammatory response that maybe attributed to their microscale features and exhibit worse osteogenic properties [18-22]. At the end of the 20th century micrometer topographies were fabricated in a controlled way to be tested with a variety of cells. In the 21st century the interest has mainly shifted towards the fabrication of nanosized topographies and different fabrication approaches have resulted in different topographies. Such fabrication methods include electron beam lithography (EBL), nanoimprint lithography (NIL), focused ion beam lithography (FIBL), laser interference lithography (LIL) and two photon polymerization technique (2PP) and they were initially used in the fields of optics and electronics. Nowadays, there is a huge interest in combining those fabrication techniques with biocompatible and novel materials. This increasing tendency towards investigating the effect of submicron and nanoscale topographies on cells is related to the understanding of the cell adhesion mechanisms and the cellular pathways that regulate cell shape, fate and activation. Cells use cytoplasmic extensions (filopodia) that can induce cell shape changes when sensing appendages in the range of 250-400 nm. Moreover, focal adhesion formation is dependent on the scale of the topographical features and they play a crucial role on signal transduction to the cell nucleus and consequently to cell adaptation [7, 23]. Therefore, submicron scale topographies are believed to be able to induce an osteoimmunomodulatory effect.

The current research is taking advantage of those advances in the nanofabrication field and explores the effect of pillar topographies, fabricated via two photon polymerization 3D printing

technique, on macrophage cell response. More specifically, the effect of six different submicron pillar topographies, differing regarding pillar interspace (pitch) and pillar height, on murine macrophages' (J774A.1) viability, morphology, attachment and phenotype polarization at different timepoints, is investigated in a systematic way.

Page intentionally left blank

Page intentionally left blank

2 Materials and Methods

The experimental methods and the equipment used along the project are in detail described in the current chapter. These include the fabrication method of the patterns as well as the methods used for their geometrical characterization. The biological part of the project is described, and the protocols developed and optimized in the laboratory for the purpose of the current project are provided in the subsections to follow. Complementary information and data sets can be found in the corresponding Appendix sections.

2.1. Fabrication of the patterns

The fabrication method of the patterns is called "Two photon polymerization method" and the equipment used is the Nanoscribe's Photonic Professional GT laser lithography system (Nanoscribe, Germany) (Figure 2). The principle of this method lies upon the fact that by focusing infrared ultrashort laser pulses onto a photosensitive material, polymerization of the material in extremely small volumes, called voxels, is possible. The system's femtosecond laser has a center wavelength of 780 nm, a pulse duration of 100 fs and a repetition rate of 80 MHz The polymerization is dependent on the laser spot-size, the laser source power and the properties of the photosensitive material. The overall quality of the fabricated structure also depends on the pre-processing and post-processing of the substrate as well as on the environmental conditions (temperature, humidity, UV exposure). The Nanoscribe system offers 2 different laser printing modes and 4 different photosensitive resists. For the investigated patterns the Conventional Direct Writing Laser (DWL) mode was used in combination with a commercially available acrylate-based photosensitive resist, known as IP-L780 and the high numerical-aperture aperture oil-immersion objective 63x (N.A=1.4). The resist was chosen because of its high-resolution printing properties and low shrinkage.

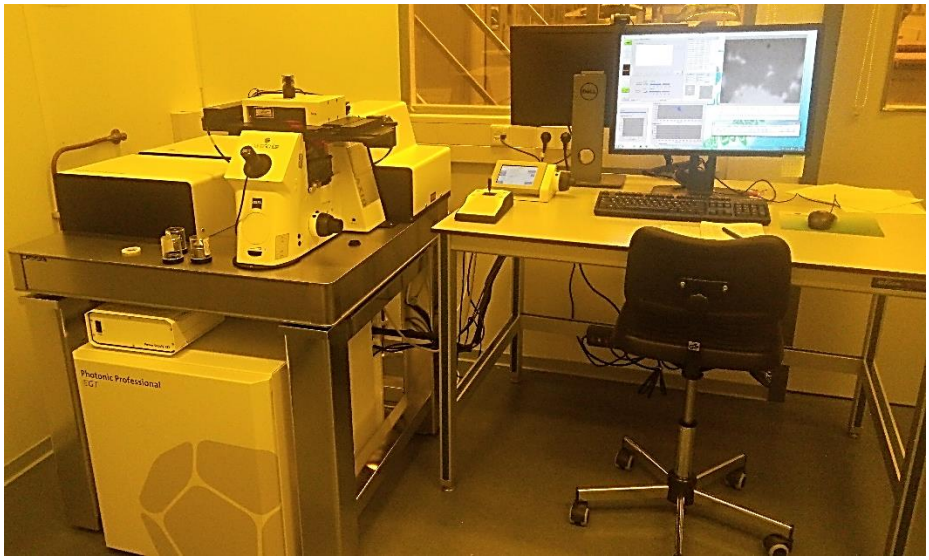

Figure 2: Nanoscribe Photonic Professional (GT) laser lithography system at the Micro- and Nano-engineering department (MNE) of the Mechanical, Materials and Maritime Faculty (3ME) of the TU Delft.

The flowchart depicted in Figure 3 gives an overview of the sequence of the actions taken to create the investigated-to-be patterns. In the following subsections each of the steps followed are described.

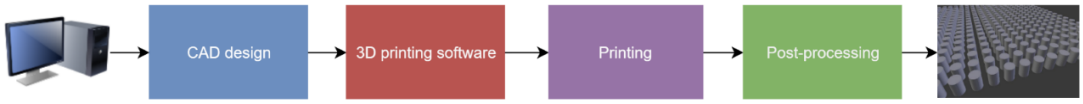

Figure 3: Patterns' fabrication process

2.1.1 CAD Design

There were different ways investigated for the design of the patterns. A variety of patterns were created using Solidworks as well as Blender software. The main component of all patterns was a single cylinder. Initially, it was attempted to create a full array of cylinders in the Blender software. Blender is a computer graphics software that enables the rendering of complex designs from Python scripts. The disadvantage of this approach lied upon the extremely high computational requirements of the software for the creation of big arrays of cylinders that could not be accommodated in the context of the current project. Therefore, the alternative approach was to design the single cylinder in the Solidworks and use the compatible 3D printing software to create the arrays needed. Six individual patterns were designed for fabrication, whose intended geometrical characteristics after fabrication are listed in Table 1 and a schematic representation of them is depicted in Figure 4. The rest of the created designs in the Blender software, together with the corresponding Python code can be found in Appendices A1 and A2.

Table 1: Characteristics of the six nanostructured patterns.

Pattern	Pillar diameter (nm)	Pillar pitch (nm)	Pillar height (nm)
P1	250	700	300
P2	250	700	500
P3	250	700	1000
P4	250	1000	300
P5	250	1000	500
P6	250	1000	1000

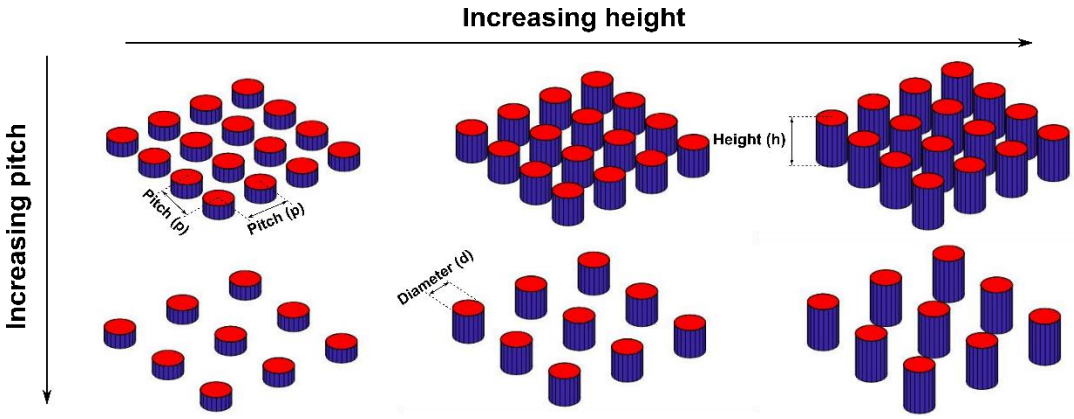

Figure 4: Pillar pitch(p), pillar diameter (d) and pillar height (h) in a schematic representation. Pillar pitch (p) is defined as the center-to-center pillar distance in the xy-plane.

2.1.2 3D printing software – DeScribe

As already mentioned, laser lithography was used to create the patterns. The system includes the hardware (Figure 2) and the software. The special editing software is called DeScribe and it is part of the system. The design can be modified, enhanced and prepared for printing through the DeScribe software. Therefore, the single cylinder created in Solidworks was saved in .stl format and imported to the DeScribe editing software and multiplied, arrays were created, the height of the cylinders was scaled, the slicing and the hatching of the cylinders were specified

as well as their pitch. The job file was then saved in .gwl format, a Nanoscribe's proprietary General Writing Language format compatible with the printer. Regarding the specific parameters applied for the fabrication of the patterns, the were optimized in the context of a previous study and therefore used as given [24]. The scanning speed was set at 1200 μm/sec and the laser power at 14% of the total laser power, the slicing (minimal distance between two adjacent planes) was set at 0.05 μm and the hatching (later distance between two adjacent lines) was set at 0.05 μm at a hatching angle of 60°. Each pattern was designed to be a square 0.5 mm x 0.5 mm consisting of pillar arrays.

2.1.3 Printing - NanoWrite

The job file in .gwl format was then imported in NanoWrite, the user-interface for the controlling of the system and the direct laser printing process. The NanoWrite gives the opportunity to monitor the system status and the printing progress because of its user-friendly interface. This step also consists of the sample preparation for printing. Commercially available glass coverslips (Menzel Glaezer, ThermoFisher Scientific, US), with a diameter of 30 mm or 12 mm and a thickness of 0.17 mm, were used as substrates for the patterns to be printed on. Some initial experiments were performed on patterns printed on the 12mm diameter glass coverslips, but the main experiments were performed on patterns printed on the 30mm diameter coverslips. There was a shift to the bigger substrates when complications with the fabrication method wouldn't allow the fabrication of the necessary number of substrates and they were also more difficult to handle during cell work. They were cleaned with acetone and wiped with a soft cloth and dried with the use of 2-Propanol (IPA) (Sigma-Aldrich, Germany) and an air-blowing gun. They were then placed and mounted with tape on the sample holder. One droplet of commercially available ZEISS Immersol 518 F optical oil was placed in the middle of the coverslip on the one side and one droplet of commercially available negative-tone photosensitive resist, known as IP-L780, on the other. The sample holder was placed in the system's stage and exposed to a femtosecond laser beam while printing. The average printing time for the patterns was 2.5 hrs.

2.1.4 Post-processing – Sample development

After the printing is completed, the glass coverslip was treated to remove the residue of the optical oil and the photosensitive resist. The coverslip was firstly immersed in 1,2-Propanediol monomethyl ether acetate (PGMEA) (Sigma-Aldrich, Germany) for 25 mins and then in IPA (Sigma-Aldrich, German) for another 5 mins. Lastly, the sample was dried using an air-blowing gun and was ready to use.

2.2. Pattern characterization

The submicron-scale surface topography of the investigated samples was evaluated both with an optical and a SEM. The optical images were used to macroscopically evaluate the homogeneity of the printed pattern before each experiment was performed with a Keyence Digital Microscope VHX-6000 (Keyence, Japan). The uniformity of the patterns was assessed by extracting the histogram of each picture using ImageJ [25]. The histogram of a picture shows the distribution of the picture pixels along the grayscale, or else the pixel intensity of each colour tone in the grayscale. The lowest the dispersion of the histogram, the highest the uniformity of the picture. The dispersion was evaluated by calculating the Coefficient of Variation (CV) for each histogram and uniformity of the pattern was guaranteed when CV < 10%. A full geometrical characterization of the patterns was performed with a Helios NanoLab™ 600i (ThermoFisher Scientific, US. The samples were gold sputtered for 40 secs using a JFC-1300 "Auto Fine Coater" (JEOL, Japan) before SEM. The geometrical features that were screened to ensure geometrical repeatability of the structures were the height, the pitch and the diameter of the pillar structures. The screening was performed in ImageJ by taking measurements of the

pillar diameter, pitch and height from different areas for all patterns. The pictures were acquired with a tilt of 30 °. The calculations were based on a minimum of 36 measurements and on a maximum of 45 measurements per geometrical characteristic.

2.3. Cell pre-culture – Seeding

The cell pre-culture conditions and seeding cell density was experimentally investigated following existing cell handling protocols and adapted to the murine J774A.1 cell line. Murine J774A.1 macrophage cells (Merck KGaA, Germany) were confluent after 3 days in 75 cm^2 flasks (Greiner Bio One GmbH, Austria) with 20 ml Dulbecco's Modified Eagle's medium (DMEM) containing 9% (v/v) fetal bovine serum and 0.9% of penicillin-streptomycin (#31966021,ThermoFisher Scientific, US) under 0.8% O_2 and 4.8% CO_2, at 37 °C at an initial cell density of approximately $7x10^5$ cells. The cells were passaged every 3rd day up to passage 15 and were frozen in vials of 1ml at a cell density of 10^6 cells/ml. All experiments were performed starting by thawing 1ml of the frozen cells, culturing for 3 days to confluence and used in the experiments at passage 16. The cells were seeded on the substrates at a cell seeding density of $5x10^4$ cells/ml and the culture media volume was 2ml. When seeded the medium was changed every two to three days, depending on the experiment. The preculturing and seeding protocols can be found in Appendices B1 and B2.

2.4. Viability

The cell viability was investigated on the patterns by live/dead staining (LIVE/DEAD™ Viability/Cytotoxicity Kit #L3224, ThermoFisher Scientific, US) after 48 hrs from seeding. The aim was to ensure that the material from which the patterns are fabricated as well as the pattern is not cytotoxic to the cells. Ethidium homodimer 1 (eth-1) and calcein AM assays were employed to evaluate the number of live and dead cells. Eth-1 is a membrane-impermeable fluorescent dye which binds to the DNA of cells with a disrupted cell membrane, thus dead cells. Calcein acetoxymethyl (AM) on the other hand, binds to the cellular membrane and can be transported inside the living cell where it becomes green fluorescent after the acetoxymethyl is hydrolysed by intracellular esterases. Cells were seeded on 1 pattern at a cell seeding density of 50,000 cells/ml and on 3 patterns at a cell seeding density of 15,000 cells/ml and incubated for 48 hrs in DMEM. After 48 hrs they were incubated for 30 mins in a 2ml phosphate-buffered saline (PBS) dilution of calcein AM (1.5 µL/ml) and eth-1(0.1 µL/ml) per well. Later, the calcein AM/eth-1 dilution was discarded and replaced with phosphate-buffered saline (PBS) for the cells to be imaged in the ZOE Fluorescent Cell Imager (BioRad, US). Live cells gave a bright green signal, whereas dead cells gave a yellowish signal. The step-by-step live/dead staining protocol can be found in Appendix B3.

2.5. Evaluation of the cell morphology

The cells' morphology was investigated with actin staining after 24 hrs of cell culturing on the patterns and consequent SEM imaging. Two experiments were performed with each one including 2 replicates of each pattern and flat control. Therefore, 4 samples per pattern and flat control were used for the quantification of the cell morphology. The actin filaments were stained with rhodamine-phalloidin, a peptide that binds to all actin filaments. For the actin fluorescent staining assay the DMEM culture medium was discarded and washed twice with phosphate-buffered saline (PBS) and consequently fixed with 4% paraformaldehyde (PFA) solution for 15 mins in room temperature. The cells were then washed with PBS and permeabilized with 0.5%Triton/PBS solution for 15 mins at 4 °C. Afterwards, the cells were blocked with 1% Bovine Serum Albumin (BSA)/PBS, incubated at 37 °C for 5 mins and stained with rhodamine-phalloidin (1:100) in 1% BSA/PBS for 1 hr at 37 °C. After washing-off the excess rhodamine-

phalloidin with 0.5%Tween/PBS and PBS, the samples were mounted on microscope glass coverslips with 10 μL of anti-fade prolong gold containing DAPI staining (nucleus staining) and were imaged at the BioRAD ZOE Fluorescent Cell Imager (BioRad, US). The number of nuclei on the patterns and around the patterns were imaged by the DAPI staining whereas the cell morphology was based on the actin staining with rhodamine-phalloidin. Moreover, after fluorescent imaging, the cell morphology was also evaluated with SEM. The samples were unmounted from the microscope glass coverslips and washed with PBS twice and incubated with 50%, 70% and 96% ethanol for 20 mins, 20 mins and 5 mins respectively. They were left to dry overnight and then gold sputtered for 40 secs using a JFC-1300 "Auto Fine Coater" (JEOL, Japan) They were imaged in a Helios NanoLab™ 600i (ThermoFisher Scientific, US). The step-by-step cytoskeleton staining protocol as well as the SEM preparation protocol can be found in Appendices B5 and B6. The morphological assessment of the cells was based on the computation of their aspect ratio performed with ImageJ using the fluorescent images. The aspect ratio calculation was performed on ImageJ and is defined by the ratio of the major over the minor axis of elongation for each cell. The aspect ratio threshold for the classification of the round and long cell morphologies was set at 1.8. For the cell morphology evaluation cell clusters were neglected and only single cells found on patterns and on the flat controls were included. The minimun number of cells evaluated for each pattern was 86 and the maximum was 303.

2.6. Immunofluorescent dual-staining

The phenotype changes induced by the patterns on the macrophages were investigated by immunofluorescent staining assays. Immunofluorescence (IF) is the method employed on biological material aiming to detect antigens using fluorescently marked antibodies. IF is widely used in cell biology labs for the detection of specific molecules in a variety of fixed cells and tissues and the main key of the method is the specificity of the antigen-antibody binding. Two different IF assays exist, the direct and the indirect IF. In the direct IF assay the antibody is covalently linked to a fluorescent dye and by the time it binds to the antigen's epitope, whereas in the indirect IF assay the antibody is first bound to the antigen's epitope and in a second step it is bound to the fluorescent dye or to the so-called fluorophore (Figure 5) [26].

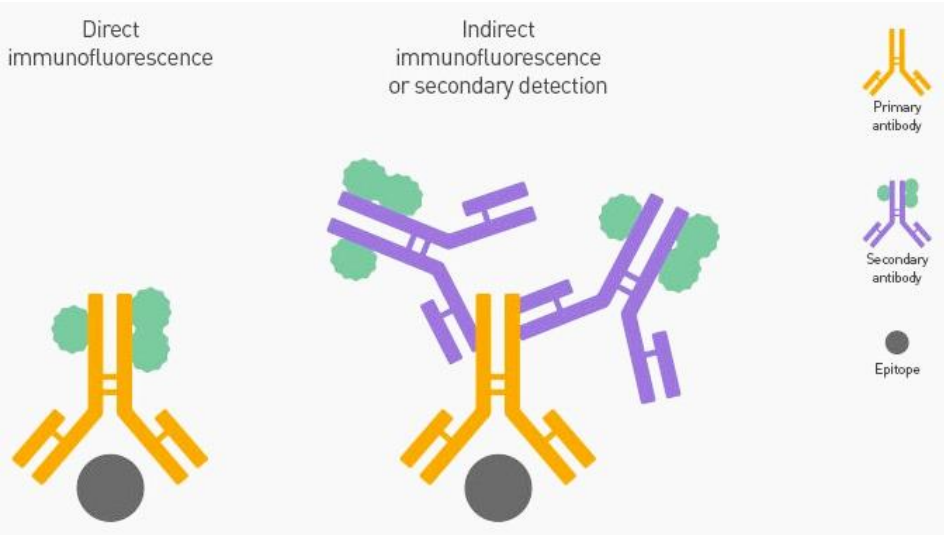

Figure 5: Direct and indirect immunofluorescence mechanism. In direct immunofluorescence (left), the antibody (yellow) is covalently bond to the fluorescent dye (green) by the time it binds to the antigen's epitope. In indirect immunofluorescence (right), the antibody (yellow) is firstly bound to the antigen's epitope and at a second step, the fluorescent dye (purple) is bound to the antibody [27].

The first combination is the iNOS/ARG-1 staining, and it was chosen based on the importance endocytic arginine catabolism. Arginine is an important amino acid deriving from protein breakdown (dietary intake) as well as from the endogenous processes like the glutamate-to-ornithine pathway [28]. It is important to note that metabolic processes are dependent on each other, forming a closed loop system to ensure effective and timely production or/and breakdown of nutrients but in the context of the current project those dynamic relationships are not going to extensively be analysed. Endocytic breakdown of arginine takes place either with the catalytic mediation of arginase, a manganese metalloenzyme, and results in the production of ornithine and urea. On the other hand, the presence of Nitric Oxide Synthases (NOS) results in the production of citrulline and nitric oxide (NO) (Figure 6). Ornithine provides a substrate for the formation of polyamines and proline. Polyamines are necessary for cell growth and differentiation whereas proline is involved in collagen formation and wound healing. NOS is a family of isozymes related to different functions with NOS-1 serving as neurotransmitter present at the peripheral nervous system, NOS-2 is related to inflammation and immune response and NOS-3 to vasodilation [29]. NOS-2 or iNOS together with ARG-1 are widely used as macrophage phenotype biomarkers with iNOS ensigning the M1 phenotype and ARG-1 the M2 phenotype.

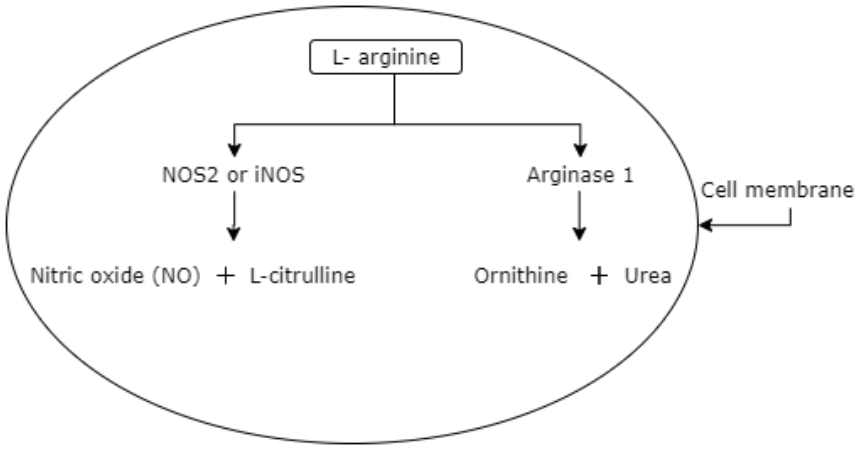

Figure 6: Intracellular L-arginine catabolism. L-arginine is catabolized to ornithine and urea with the catalytic mediation of arginase 1 or at the presence of iNOS it is catabolized to NO and L-citrulline [30].

The second combination is staining for the CCR7/CD206 biomarkers. CCR7 is a protein encoded by the CCR7 gene and belongs to the G protein-coupled receptor family. In mice the positioning of this gene is found in the 11th chromosome and the CCR7 receptor is said to activate B and T lymphocytes and to be expressed in lymphoid tissues [31]. The chemokines belonging to the G protein-coupled receptor family have 7 transmembrane domains and they serve at transmitting signals from the extracellular environment inside the cell. CCR7 is reported to be a M1 macrophage phenotype biomarker due to its involvement with inflammatory processes. CD206 or mannose receptor is a transmembrane calcium-type protein found in macrophages amongst other cell types. It is involved in the regulation of the inflammation by controlling the levels of glycoproteins in the circulation. At the inflammatory phase the mannose receptor stays mostly unexpressed, whereas at the non-inflammatory state its expression is increased [32]. Consequently, CCR7 is used to identify M1 polarized macrophages and CD206 for M2 polarized macrophages [33].

The step-by-step phenotype staining protocols that were used can be found in Appendices B4 and B5. In short, for both staining assays the DMEM culture medium was discarded after 24h of cell culturing on the patterns and the cells were washed twice with phosphate-buffered saline

(PBS) and consequently fixed with 4% paraformaldehyde (PFA) solution for 15 mins in room temperature. Another washing step with PBS was employed and the macrophages were permeabilized with 0.5% Triton/PBS solution for 15 mins at 4 °C. Afterwards, they were blocked with UltraCruz (sc-516214, Santa Cruz, US) for 15 mins at 37 °C. The primary antibodies for NOS2 (sc-7271, Santa Cruz, US) and anti-liver Arginase (ab91279, Abcam, UK) were diluted in UltraCruz at a concentration of 1:100 and incubated overnight at 4 °C. For the CCR7/CD206 staining, the blocking step was performed with 1% BSA/PBS and the primary antibodies for CCR7 (ab32527, Abcam, UK) and CD206 (ab8918, Abcam, UK) were diluted in 1% BSA/PBS at a concentration of 1:100. The next day, excess antibody was washed off with 0.5%Tween/PBS in multiple steps and the secondary Alexa-Fluor 488 (#10544773, ThermoFisher Scientific, US) and Alexa-Fluor 594 (#10798994, ThermoFisher Scientific, US) were diluted in the UltraCruz blocking agent for the iNOS/ARG-1 at a concentration of 1:100 and in 1% BSA/PBS for the CCR7/CD206 staining group at 1:50 for Alexa-Fluor 488 and 1:150 for Alexa-Fluor 594. The incubation took place at room temperature for 1 hour and the samples were kept in the dark to avoid fading-off of the fluorescent capacity of the antibodies. Afterwards, the samples were washed with PBS for 5 mins at room temperature and were mounted on microscope glass coverslips with 10 μL of anti-fade prolong gold containing DAPI staining (nucleus staining). Imaging was performed at ZOE Fluorescent Cell Imager (BioRad, US) for the iNOS/ARG-1 couple (results not presented here) and on a ZEISS LSM 900 (ZEISS, Germany) for the CCR7/CD206 couple. 3 experiments were performed regarding the expression of the CCR7/CD206. In the first one, macrophages were seeded on the patterns for one day before being stained for CCR7/CD206. In the second and third one, macrophages were initially polarized to M1 phenotype following the protocol in Appendix C, and subsequently seeded on the patterns for one day before staining for experiment two and for three days before staining for experiment 3. This was an attempt to evaluate different timepoints and conditions and to explore the effects of the patterns on the macrophages. The assessment of the CCR7/CD206 levels was done by means of image processing of the fluorescent images. The average intensity for each substrate and biomarker in each experiment was extracted from the histogram of the fluorescent images, considering only single cells and disregarding clusters of them. The minimum number of cells accessed per pattern for the earliest timepoint (day 1) was 24 and the maximum was 171, whereas for the latest timepoint (day 3) the minimum number of cells was 169 and the maximum was 381.

2.7. M1/M2 macrophage polarization – Positive control group

To reliably access the effect of the fabricated patterns on the J774A.1 a positive control group had to be created to eliminate any chance of misinterpreting the results. To do so, J774A.1 macrophages had to be stimulated to express their M1 and M2 phenotype. As mentioned already in the introduction of the current dissertation, macrophages express their inflammatory behaviour, M1, when exposed to LPS and INF-γ, whereas they switch to the M2 phenotype in the presence of IL-4. Evidently, those were the substances used to stimulate the macrophages. Based on literature a concentration of 100ng/ml of LPS and 10 ng/ml of INF-γ and 72hrs of stimulation could result in M1 polarization of the J774A.1 macrophages, and a concentration of 10ng/ml IL-4 and 72hrs of stimulation could result in M2 polarization of the cells [34]. More experiments were carried out with four different LPS concentrations and 3 different stimulation durations aiming to detect the best possible scenario of stimulation. The cells were stained for the expression of iNOS/ARG1 that showed vague M1 macrophage presence. The results and experimental design are presented in Appendix C. To validate the results another pair of biomarkers, the CCR7/CD206 were used as well as a Griess assay test. Hence, 50.000 cells/well were seeded on the glass slides and cultured with DMEM containing 100 ng/ml of LPS (L4391, Sigma-Aldrich, Germany) and 10 ng/ml of INF-γ (I4777, Sigma-Aldrich, Germany)

for 72hrs for the first control group and the same cell seeding density was used to for the M2 stimulation by adding 10ng/ml IL-4 (SRP3211, Sigma-Aldrich, Germany) to the DMEM culture medium. The test was performed in duplo for each positive control group. The M1/M2 macrophage polarization was followed by immunofluorescent staining for the phenotypes the biomarkers CCR7/CD206 and the nitrite concentration in the cell supernatant was accessed with Griess assay.

2.8. Non-specific binding of secondary antibodies

For the validation of the staining protocol, another experiment was carried out aiming to investigate any non-specific binding of the secondary antibodies on cell receptors without the presence of primary antibodies. The process followed started by discarding the DMEM culture medium and by double washing of the cells with phosphate-buffered saline (PBS) and consequent fixation with 4% paraformaldehyde (PFA) solution for 15 mins in room temperature. After fixation, the cells were washed with PBS and they were permeabilized with 0.5% Triton/PBS solution for 15 mins at 4°C. In the blocking step the cells were incubated with 1% BSA/PBS at 37°C for 15 mins. The secondary antibodies were employed after blocking, and specifically Alexa-Fluor 488 and Alexa-Fluor 594 were diluted in 1% BSA/PBS at a concentration of 1:100. This experiment was important to ensure that the duration of blocking and the blocking agent were appropriate for this experiment.

2.9. Griess assay – NO activity

The Griess assay was tried out to test the effectiveness of the stimulation protocol for the positive control groups. The Griess test is used to evaluate the presence of nitric oxide in a solution. It is widely used as a colorimetric test to evaluate changes in the nitric oxide concentration of different solutions. The principle is based upon the diazotization reaction described by Peter Griess in 1858 (Figure 7). Solutions containing nitrite ions react with sulfanilamide, diazonium salt is formed and a pink colour is developed.

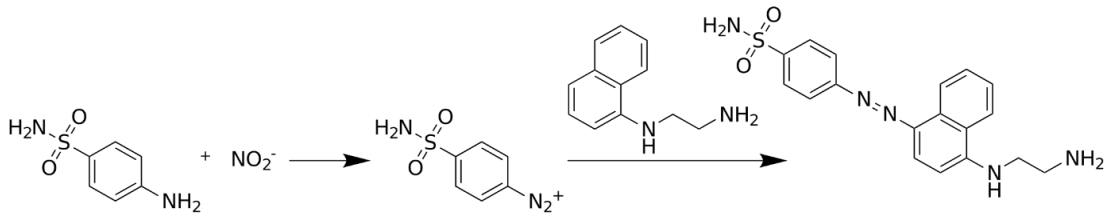

Figure 7: Griess diazotization reaction. NO_2^- ions react with sulfanilamide (Griess Reagent I) and N-(1-naphthyl)ethylenediamine dihydrochloride solution (Griess Reagent II) to form diazonium salt that gives a pink colour [35].

The Griess reagent kit used (ab234044, Abcam, UK) is a two-step test, first reducing the nitrite to nitrogen oxide and then adding a second reagent to stabilize the solution and detect the product at 540 nm. The product was measured using the VICTOR Multilabel Plate Reader (Perkin Elmer, US). This device is light-sensitive and measures the transmittance and absorbance of the light passing through the solution. The absorbance measurement is interpreted in colour intensity and therefore concentration of the nitrite ions in the solution, based on the Beer-Lambert law that correlates absorbance with the concentration of a solute in a solution [36]. The concentration of nitrite was measured in the cell culture media of the stimulated macrophages with LPS/INF-γ and IL-4 as well as with pure DMEM. 250 μL of the culture medium were collected and put in vials. They were spinned down to 1000 x g for 15 mins and the supernatant was collected and 100 μL were pipetted in a microplate in duplo. Initially, 10 μL of the first Griess reagent was added to the wells followed by the addition of 10

μL of the second Griess reagent. The wells' volume was adjusted to 200 μL by adding 80 μL of the nitrite assay buffer solution. The samples were incubated for 10 mins at room temperature while being mixed using a shaking platform. The absorbance was read at 595 nm within 60 mins. The standard solution and standard curve concentrations were prepared according to the manufacturer's manual (Appendix D).

2.10. Statistical analysis

Different statistical methodologies were applied to access a variety of parameters in the current project. The assessment of the cell number on the patterns compared to the surrounding substrate was performed by analysis of the images obtained after the cytoskeleton and nucleus staining with ImageJ [25]. Initially the data collected was accessed on normality. It was found that they did not follow normal standard Gaussian distribution for all patterns. Therefore, the number of the nuclei on the patterns and on 4 different areas of the same size were counted and compared using non-parametric one-tailed Mann-Whitney test for the groups that were not normal and the Welch's t-test for the groups that were normal. Statistically significant differences amongst the 6 different patterns were accessed with one-way non-parametric Anova. The area covered by the cells on the patterns was accessed with ImageJ and expressed as a percentage of the patterned area. Non-parametric Kruskal–Wallis one-way analysis of variance was applied to test whether significant differences amongst the 6 investigated patterns exist. The cell size and shape were also accessed and analysed from the images obtained after the immunofluorescent cytoskeletal staining and an ellipse fitting on the single cells was performed. The aspect ratio, given by the ratio of the major/minor axis of the ellipse was used for the classification of the cells in the categories of round and elongated. Any cell with an aspect ratio larger than 1.8 was considered an elongated cell. Differences of the elongated/round cell ratios, the cell size area and single cell size on the patterns and on the flat surface were evaluated using non-parametric Kruskal-Wallis one-way analysis of variance. For the assessment of the phenotype across substrates for the two biomarkers (CD206/CCR7) separately, the non-parametric Kruskal-Wallis one-way analysis of variance for the obtained mean intensity levels was applied. To explore differences between the levels of CD206 and CCR7 per pattern, and since the groups passed the Kolmogorov-Smirnov normality test, two-way Anova was used. Statistical analyses were performed using GraphPad Prism 7.04 (GraphPad Software, San Diego, CA) and a $p<0.05$ was considered statistically significant and indicated with a single asterisk (*), $p<0.01$ was indicated with a double asterisk (**), $p<0.001$ with a triple asterisk (***) and $p<0.0001$ with four asterisks (****).

Page intentionally left blank

3 Results

The outcome of the previously described experimental procedures are presented in this chapter. These include the geometrical characterization of the fabricated patterns, cell viability results, results about the cell morphology on the patterns as well as the phenotype polarization of the J774A.1 cells mediated by the investigated patterns.

3.1. Geometrical characterization of the patterns

In the current paragraph the measured geometry of the patterns is going to be presented. Representative images of the patterns used in the course of the research are also included.

3.1.1. Optical microscopy

Every sample produced and used in the experiments was imaged with an optical microscope. The reason is to have a macroscopic visualization of flaws and differences amongst the utilized patterns. In 3D printing techniques variation in the quality of the fabricated features is a common issue and in order to ensure consistency in the analysis of the results it is of great importance to know how the patterns exactly look. Optical images of the patterns are depicted in Figure 8.

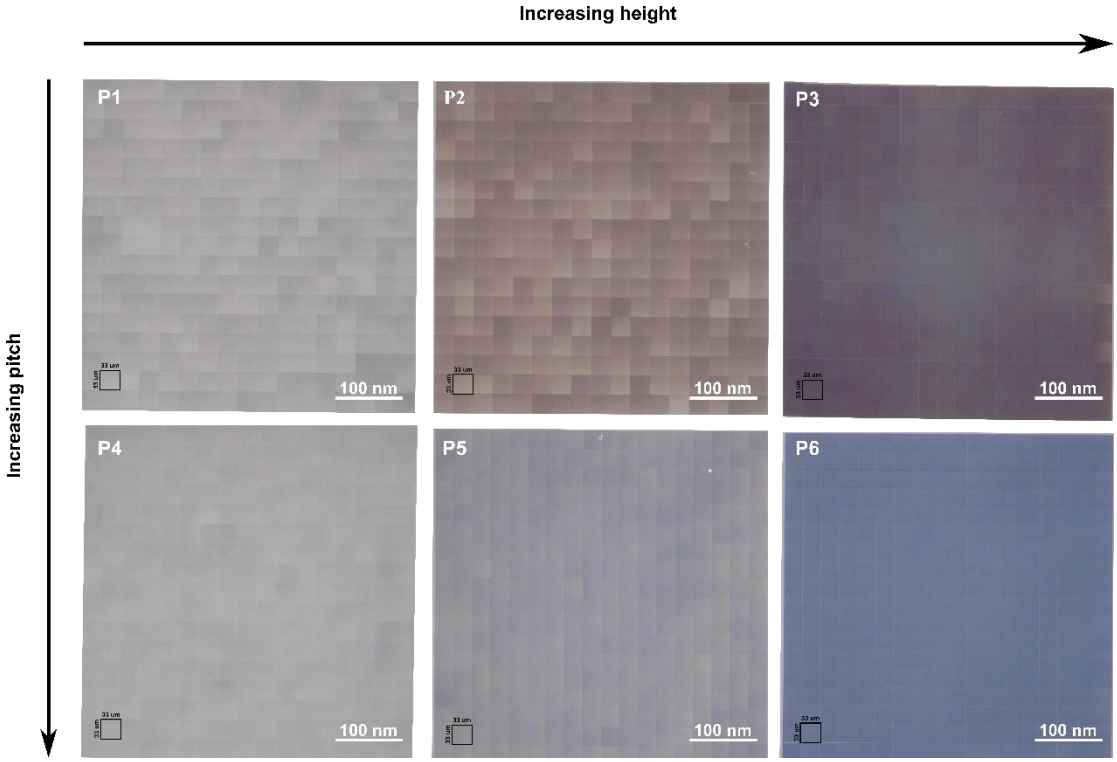

Figure 8: Optical microscope pictures of the investigated patterns P1 to P6 in ascending order of pillar height and pillar pitch. The printed area for each pattern was a 0.5 mm x 0.5 mm square with a writing field of 0.33 μm x 0.33 μm square.

The uniformity of the patterns was assessed by investigating the histogram of each picture. The CV was calculated, and it was shown that the patterns are very uniform with CV values below 10%.The histograms and CV values are depicted in Figure 9. In Figure 10 the mean and standard deviation for the pixel intensity diagram of each pattern is presented. The standard deviation is very small for all patterns and the mean grayscale value indicates that the patterns the denser and higher the pillar array, the “darker” the image.

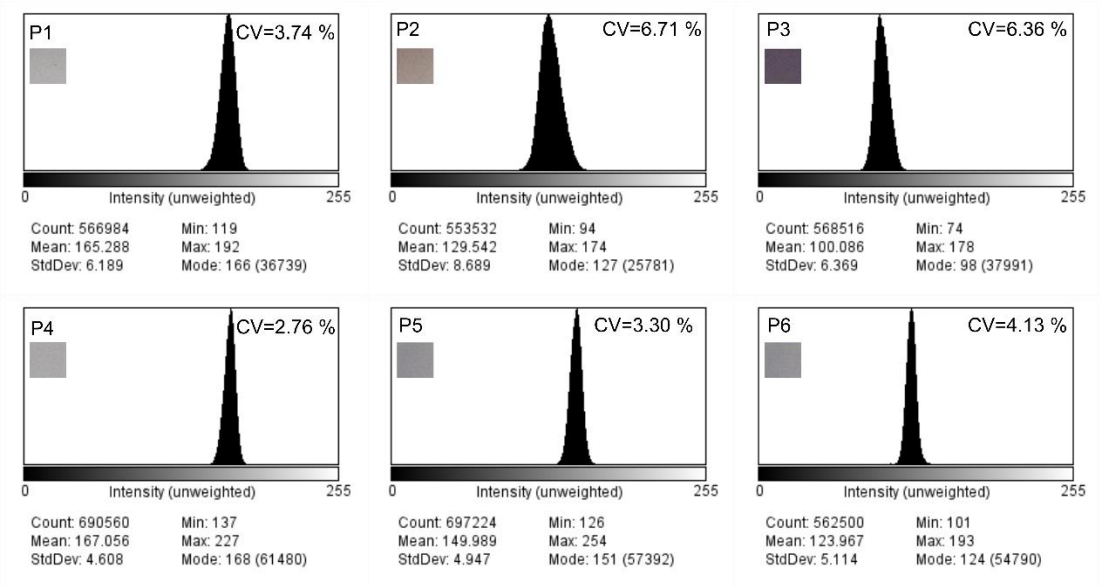

Figure 9: Histograms of the optical images for the 6 investigated patterns. Uniformity assessment was based on the pixel intensity of the colour tone of each pattern. The mean and standard deviation for each histogram are reported. Coefficient of variation (CV) is reported for each pattern, showing the variability related to the mean of population.

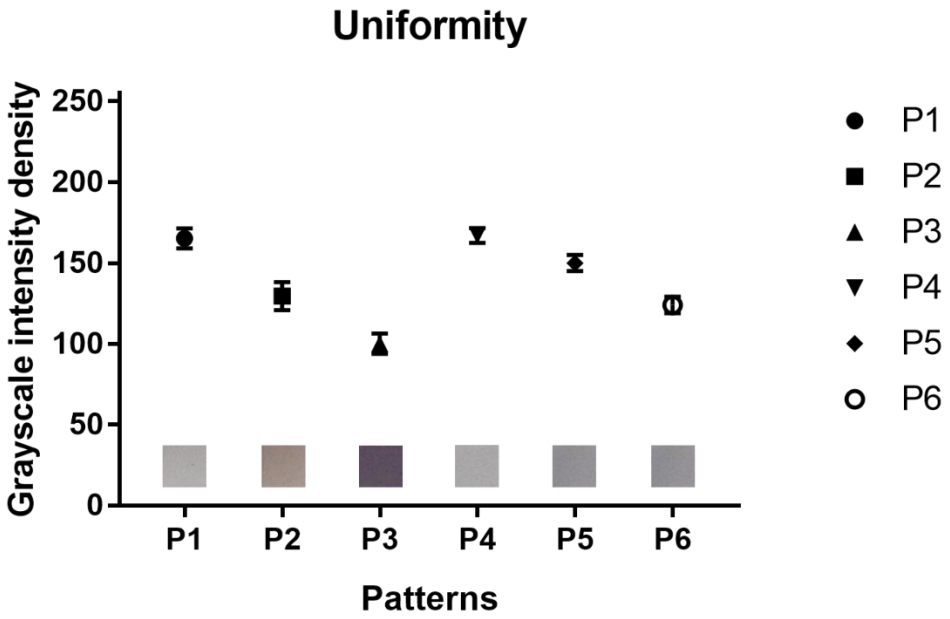

Figure 10: Uniformity of the patterns based on the grayscale pixel intensity of the images obtained with the optical microscope. Pixel intensity expressed with a mean and standard deviation.

3.1.2. Scanning electron microscopy

The geometrical characteristics of the patterns were investigated with SEM (Figures 11 and 12).

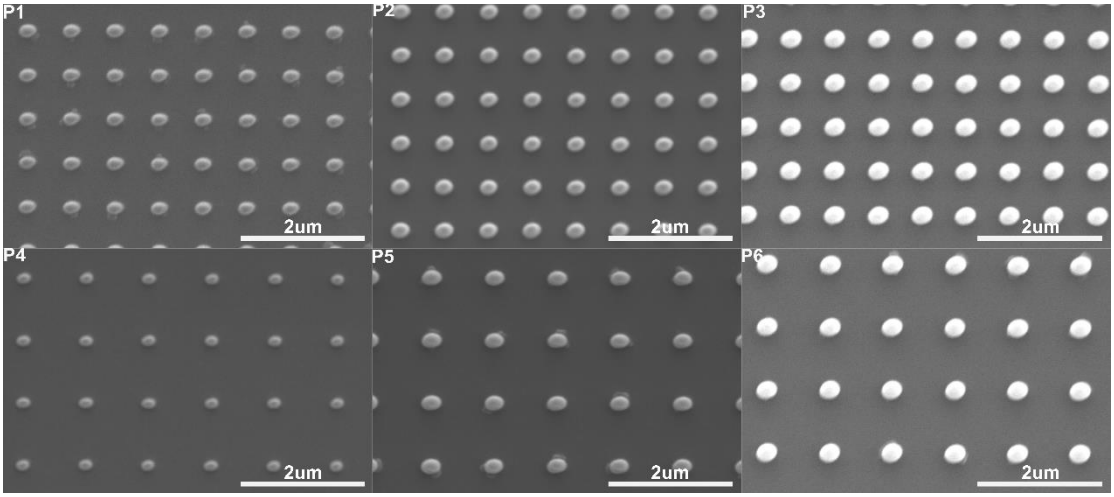

Figure 11: SEM top view images of the six investigated patterns fabricated in Nanoscribe Photonic Professional GT (scale bar: 2 µm).

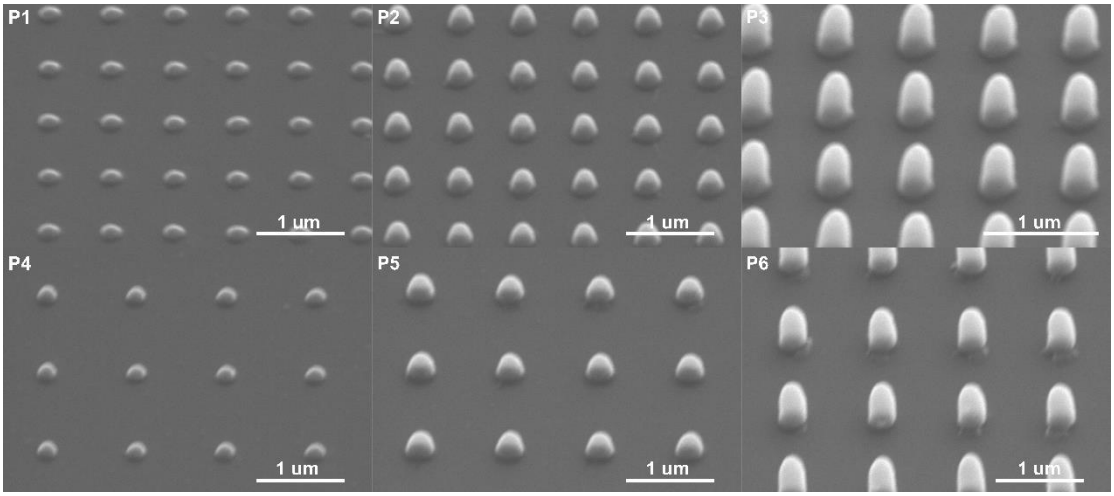

Figure 12: SEM 30° deg angle images of the six investigated patterns fabricated in Nanoscribe Photonic Professional GT (scale bar: 1 µm).

A quantitative analysis of the pillar diameter, height and pitch was performed, and the results are summarized in a table in Appendix E. Figure 13 presents the comparison of the measured pillar pitch, diameter, height and aspect ratio relative to the nominal values. The pillar pitch measurements show very little variation compared to the designed 700 nm and 1000 nm pitch. As far as the pillar diameter is concerned, there are variations with respect to the designed 250 nm pillar diameter that are however not statistically significant. The fabricated pillar height also shows some variation compared to the designed height for the pillar height of each pattern, however the variations are not statistically significant.

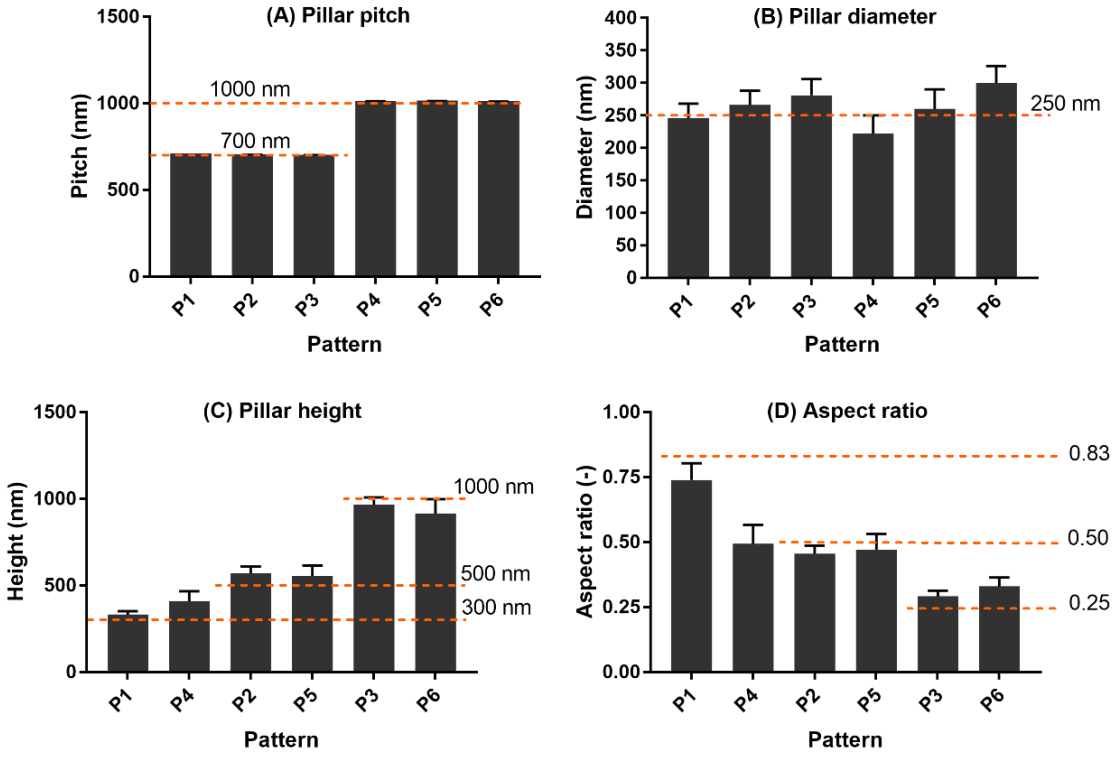

Figure 13: Geometrical characteristics of the patterns as measured (columns) compared to the nominal values (dotted lines). (A) Pillar pitch, (B) Pillar diameter, (C) Pillar height, (D) Aspect ratio.

3.2. Cell viability

The cell viability results (Figure 14) showed that the material the pillars are made of is not cytotoxic. The viability levels of macrophages were investigated on patterns P2, P3, P5 and P6 and on a non-patterned flat coverslip by using 2 different cell densities. Patterns P3 and P6 together with a flat sample were tested at a cell seeding density of 50,000 cells/ml, and patterns P2, P5 with a flat sample were tested at a cell seeding density of 15,000 cells/ml. These tests also showed that viability levels are independent of the cell seeding density. The patterned area for all experiments was 0.5 x 0.5 cm^2. More results can be found in Appendix E.

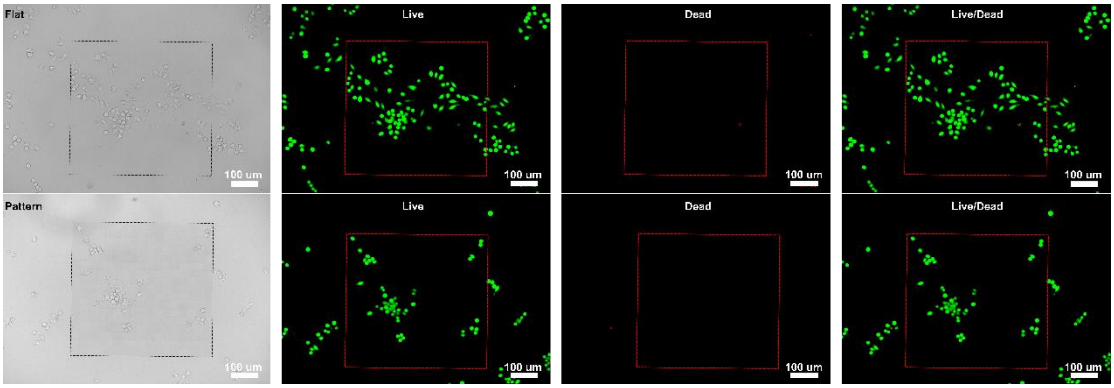

Figure 14: Live/Dead staining with cell density 15,000 cells/well. Brightfield, green channel, red channel and merged green/red channel fluorescent images (from left to right).

3.3. Cell-pattern interactions

In the current paragraph results on the cell density, the cell morphology as well as the cell polarization on the patterns are presented. Information about statistically significant differences in the cell behaviour amongst the patterns is also included.

3.3.1. Cell attachment

Figure 15 depicts the differences in the number of cells on the patterns and on the flat control after 1 day of culture. Based on the statistical analysis that was performed, the differences of the means between patterns P1 and P2 are of high statistical significance ($p<0.01$). The number of cells on the P2 pattern is also significantly higher than the number of cells on the P4 patterns with a p-value of $p<0.001$. The relationship between P2 with P6 shows that the number of cells on P2 is significantly larger that on P6 and that the difference in the numbers between P3 and P4 is also statistically significant. The relationship of P2 with P4 and P1 indicates that pillar pitch might affect cell attachment to a greater extent than pillar height. The results also show that increased pillar height may be more preferable for cell attachment, but in combination with increased pillar pitch cell attachment is inhibited. Figure 15 also shows the area the cells occupied after one day on the patterns and on the flat control surface as a percentage of the total patterned area. The area occupied by the cells on patterns P1 and P4 is significantly smaller compared to the area the cells occupy on pattern P2. This phenomenon can be explained in correlation with the number of cells on each pattern as pictured in Figure 15, hence, the higher the number of cells the larger the area they can cover while adhering and proliferating. No other significant differences were observed amongst the rest of the patterns.

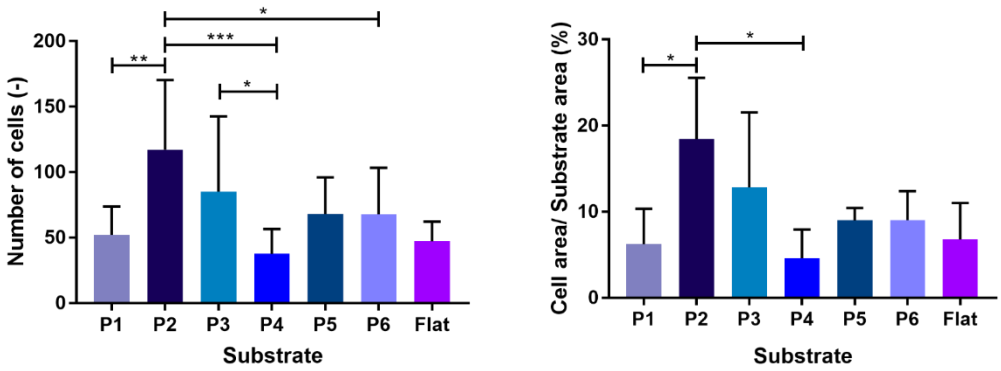

Figure 15: Number of cells per patterns (left) and area that the cells occupy as percentage of the total patterned area (right). Significant differences are indicated by the bar and the p-value. The notation for $p<0.05$ is one asterisk (*), for $p<0.01$ two asterisks (**) and for $p<0.001$ three asterisks (***).

3.3.2. Cell morphology

Macrophages exhibited two different morphologies both on the patterns and on the flat surfaces (control), namely round and elongated (Figure 16). The cells attached to the pillars by forming cytoplasmic extensions. On the flat substrate the cells looked relatively spread with numerous cytoplasmic extrusions, whereas on the patterns they seemed to be “stressed” and shrunk, extending in the vertical direction.

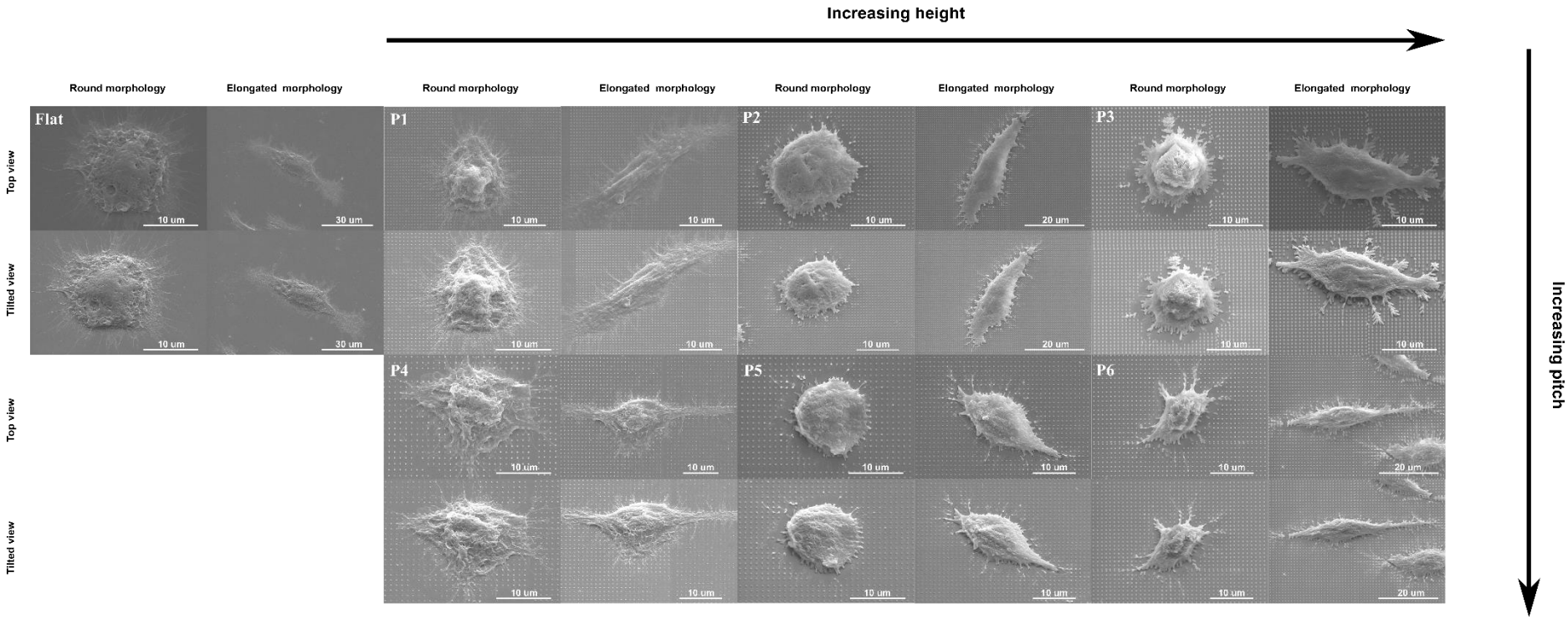

Figure 16: Round and elongated morphologies encountered per substrate. For each pattern, the upper photos are top-view images of the cell morphologies (round=left, elongated=right) and the bottom photos are tilt-view images of the same cells from a 30° angle.

Figure 17 depicts the ratio of elongated to round cells on the patterns. It is observed that with increasing height, the number of elongated cells is increasing. Moreover, the number of the elongated cells appears to be inversely proportional to the pitch size. Clearly, the highest and the denser the pillars are, the higher the cytoskeletal tension and more elongated the cells are appearing to be. It is also interesting that the patterns P1 and P4 have none or almost none effect compared to the flat surface when it comes to cell elongation.

In Figure 18 the aspect ratio of the cell, and the cell area in um^2 for both the round (left) and the elongated (right) cell morphology per substrate is plotted. For the round cell morphology, the single cell aspect ratio does not differ significantly amongst the patterns and the flat control surface. However, in the left bottom graph of Figure 18 it is shown that the single cell area differs significantly amongst the different substrates. It appears that the cell area is significantly increased on all patterns compared to the flat surface. Additionally, based on the significance levels between patterns with a pitch size of 1000 nm (P4, P5) and patterns with pitch size of 700 nm (P1, P2) with the flat surface, it appears that a pitch of 1000 nm induced higher levels of cell spread than a pitch of 700 nm. Moreover, patterns with the highest pillar height, P3 and P6 seem to induce similar effects with respect to cell spread with the flat surface.

For the elongated cell morphology, there are already statistically significant differences in the aspect ratio amongst the patterns. Firstly, elongated cells on the P3 pattern appear to be significantly longer compared to the elongated cells on P1, P2, P5, P6 and on the flat surface. This trend is also in line with the cell spread of the elongated cells, hence, elongated cells on P3 occupy larger areas that elongated cells on P1, P2 and on the non-patterned surface.

In Figure 19, close-up images of the cell attachment are presented. On P1 and P4 the cells attached to the pillars by forming thin and long filopodia. On the patterns with increasing height, thus, patterns P2, P3, P5 and P6, the cells appear to form short filopodial protrusions that not only bend, but also manage to detach the pillars. Some of these filopodial protrusions seem however, to experience rupture while detaching the pillars.

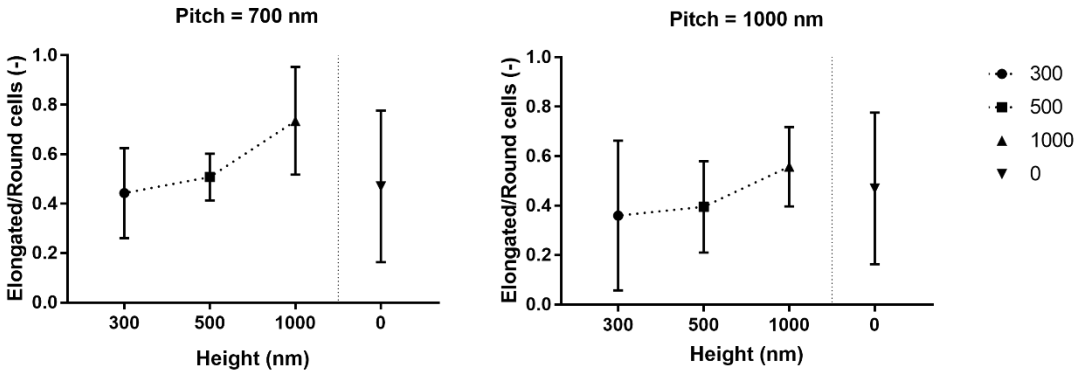

Figure 17: Ratio of elongated to round cells for the patterns with pitch = 700 nm (left) and for the patterns with pitch = 1000 nm (right).

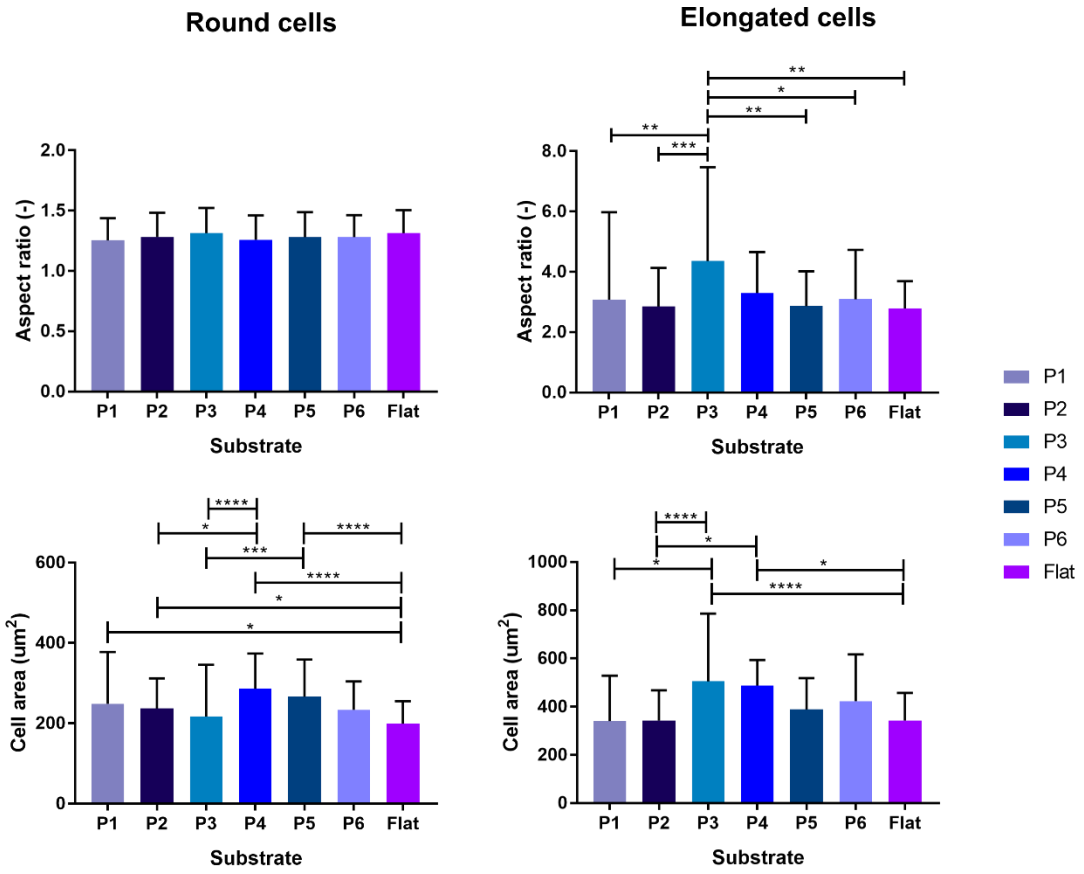

Figure 18: Round single cell aspect ratio per substrate (upper left graph). Round single cell size per substrate in um^2 (bottom left graph). Elongated single cell aspect ratio per substrate (upper right graph). Elongated single cell size per substrate in um^2. Data is presented as mean ± SD. The notation for $p<0.05$ is one asterisk (*), for $p<0.01$ two asterisks (**), for $p<0.001$ three asterisks (***) and for $p<0.0001$ four asterisks (****).

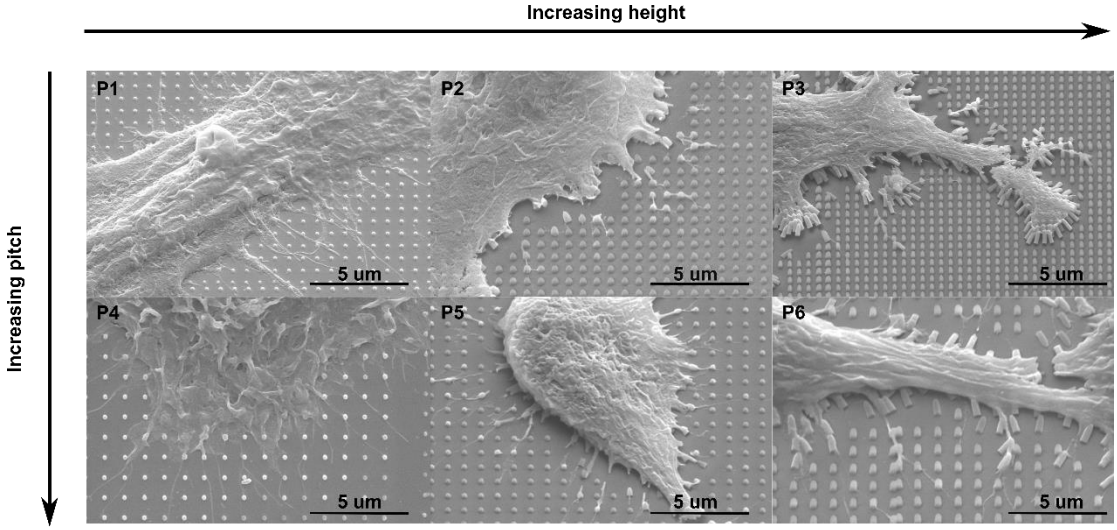

Figure 19: Details of the cytoplasmic extensions' attachment on pillars of different heights. Cytoplasmic extensions are able to detach pillars with heights >500 nm.

3.4. Cell polarization

For the assessment of the macrophage phenotype on the patterns, a staining protocol as well as a positive control had to be developed. Suitable biomarkers for the different phenotypes had to be chosen, tested and validated before the staining protocol could be employed on the patterns. Moreover, macrophages had to be stimulated to switch to the investigated phenotypes, in order to serve as a reference for the experimental results. For the validation of the staining protocol the possibility of non-specific binding of the secondary antibodies to the cells had to be tested. For the validation of the stimulation protocol, a nitrite concentration test was performed.

3.4.1 Non-specific binding results

As mentioned in section 2.8, the staining protocol was validated by investigating any possible non-specific binding of the secondary antibodies in the absence of primary antibodies. The results are presented in Figure 20 and it is clear that the secondary antibodies do not bind on cellular membranes of the cells, without a compatible primary antibody being present. This is indicated by the fact that, despite the existence of cells, whose nuclei are stained with DAPI (blue dots in the figure), there is no sign of active staining with Alexa Fluor 488 and 594. This test proves that the use of 1% BSA/PBS as a blocking agent for 15 mins in the blocking step is appropriate.

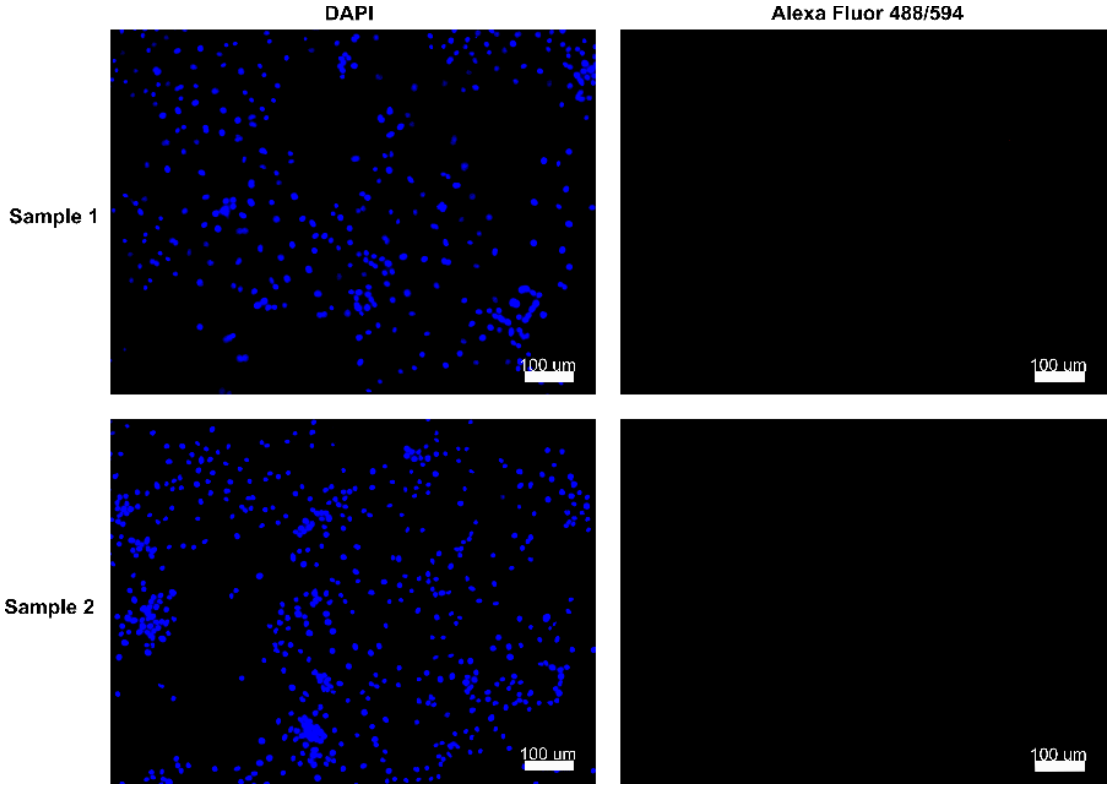

Figure 20: Omission of the primary antibody proved the specificity of the primary and secondary antibodies employed in the dual fluorescent staining. The presence of cells on the surface indicated by DAPI nuclei staining (left; blue dots), while no signal was present in the fluorescent channels for Alexa Fluor 488 and 594 (right; no signal) and non-specific binding of the secondary antibodies was negated.

3.4.2 Griess assay – Nitrite concentration result

Following the Griess assay protocol, as given from the supplier (Appendix D) and described in the paragraph 2.9, the standard curve for the nitrite amounts was plotted (Figure 21) and the measured absorbance units were fitted. The nitrite concentrations in the collected supernatant were obtained by fitting of the measured absorbance values to the standard curve and calculating the nitrite concentration by dividing the nitrite amounts (nmol) by the investigated dilution volume (ml). The results given in the table of Figure 21 show a slight increase in the nitrite concentration in the LPS/INF-γ stimulated group compared to the IL-4 stimulated and the DMEM group.

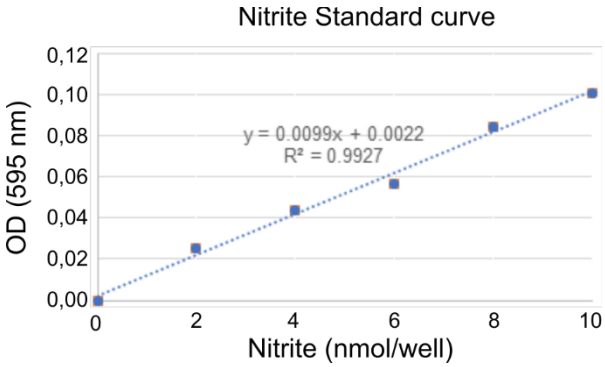

Supernatant	Nitrite Concentration (µM)
LPS/INF-γ	12.9
IL-4	12.5
DMEM	12.6

Figure 21: Nitrite standard curve and nitrite concentration in the supernatant calculated for the LPS/INF-γ and IL-4 stimulated groups and for the non-stimulated (DMEM) group.

3.4.3 M1 and M2 stimulated macrophages

Figure 22 depicts the differences between the M1 and M2 stimulated macrophages and establish the positive control of the experiment. M1 macrophages appear to be much more elongated compared to the M2 stimulated cells as well as less in numbers. Moreover, they have a CCR7 expression (red) and no CD206 expression (green). The non-stimulated macrophages have a rounder morphology, similar to that of the M2 cells but a lower CD206 expression than the M2 macrophages.

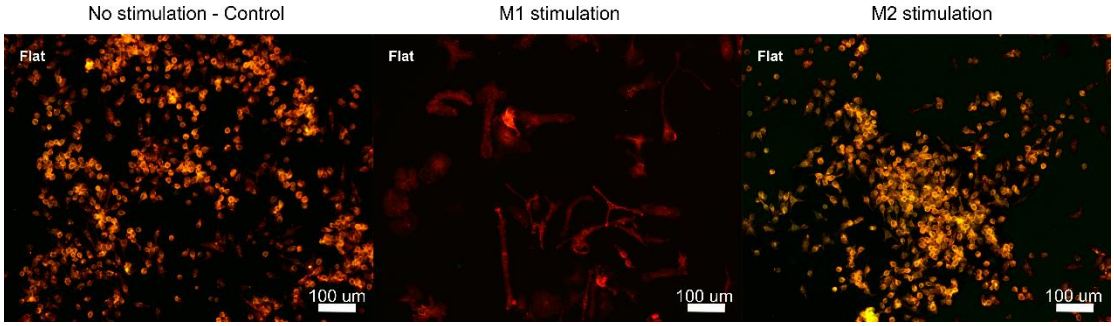

Figure 22: Immunofluorescent images for CCR7 (M1 phenotype, in red) and CD206 (M2 phenotype, in yellow) markers in adherent J774.A1 cells on flat samples after LPS/INF-γ and IL-4 stimulation for 72 hrs (Positive control).

3.4.4 Macrophage phenotype markers expression

In the current section the analysis of the immunofluorescent phenotype staining for the three different groups is presented. Figure 24, Figure 25 and Figure 26 show fluorescent images of all groups of adherent J774A.1 macrophages double stained with the M1 (CCR7:red) and M2 (CD206:green) surface markers after one day of seeding without pre-stimulation, after one day of seeding with M1 pre-stimulation and after 3 days of seeding with M1 pre-stimulation, on all investigated patterns. Clustering of the macrophages is observed on the majority of the patterns after 3 days of seeding (third group). Macrophages express both biomarkers at all cases as demonstrated in the figures and a qualitative analysis was performed to evaluate the intensity levels of the two colours and subsequently collect information about the surface markers' expression levels and the information obtained is presented in Figure 23.

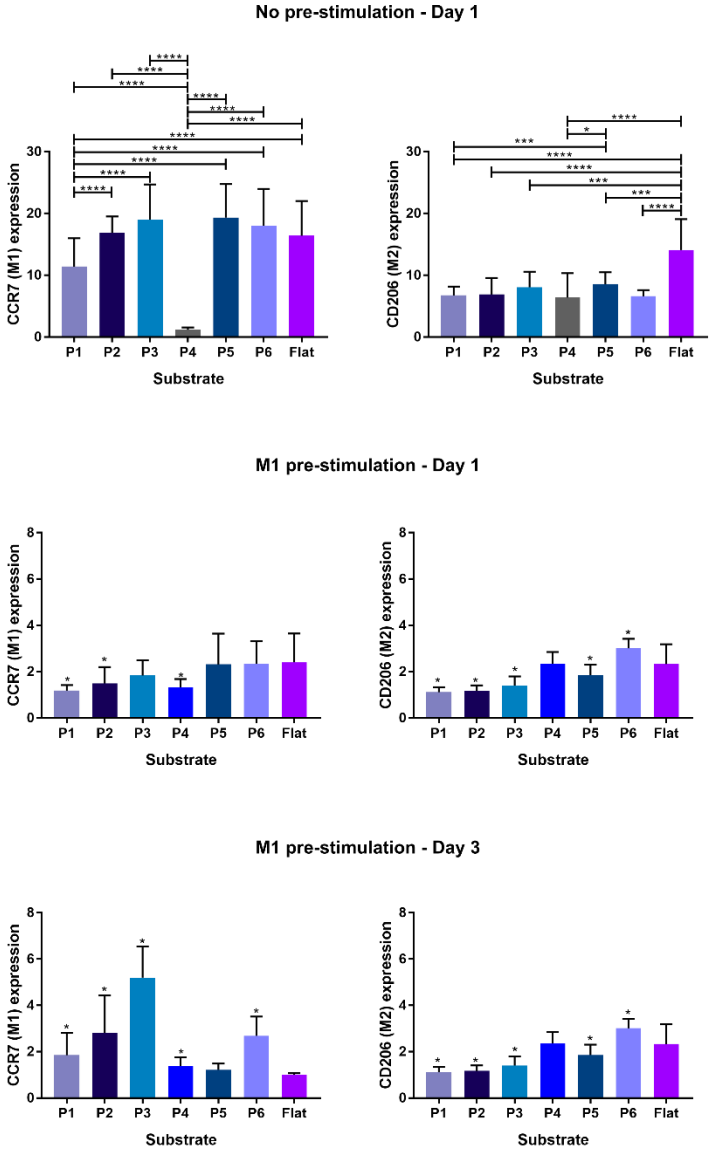

Figure 23: Results of the analysis on the grayscale intensity levels of the immunofluorescent staining dyes (CCR7: M1, CD206: M2) for the three different groups (No stimulation – Day 1, M1 population - Day 1, M1 population – Day 3). Data is presented as mean ± SD. The notation for $p<0.05$ is one asterisk (*), for $p<0.01$ two asterisks (**), for $p<0.001$ three asterisks (***) and for $p<0.0001$ four asterisks (****).

For the non-stimulated cells after one day of seeding, the M1 and M2 biomarker levels differ amongst the different substrates significantly. CCR7 expression in pattern P4 was significantly lower than on any other pattern including the flat control surface. Amongst the rest of the patterns, the one showing significantly lower CCR7 expression is pattern P1. It can be deduced that a pillar height larger than 300 nm triggers a higher CCR7 expression. On the other hand, the expression of CD206 was significantly higher on the flat surface than on any of the patterned surfaces.

For the M1-stimulated cells after one day of seeding, the M1 and M2 biomarkers showed a very specific trend. CCR7 expression is increasing with an increasing pillar height and remained at higher levels on the flat control surface. CD206 is following the same trend for the patterns with a pillar pitch of 700 nm, thus the lower the pillar height the lower the CD206 expression. CD206 expression on P4 with pitch size of 1000 nm, was at the same levels like on the flat control surface and the combination of the largest pillar pitch size with the largest pillar height (pattern P6) induces the highest CD206 expression.

After 3 days, the M1-stimulated cells showed higher CCR7 expression on almost all patterns compared to the flat surface. Moreover, a staggering CCR7 expression with staggering pillar height at a pillar pitch of 700 nm was observed. Patterns P4 and P6 induced significantly higher CCR7 expression compared to the flat surface whereas the levels of CCR7 for pattern P5 was similar to those on the flat surface. CD206 levels of expression were the highest on pattern P6 compared to the flat control surface. The lowest CD206 expression was observed on patterns P1, P2 and P3 sharing a pitch size of 700 nm.

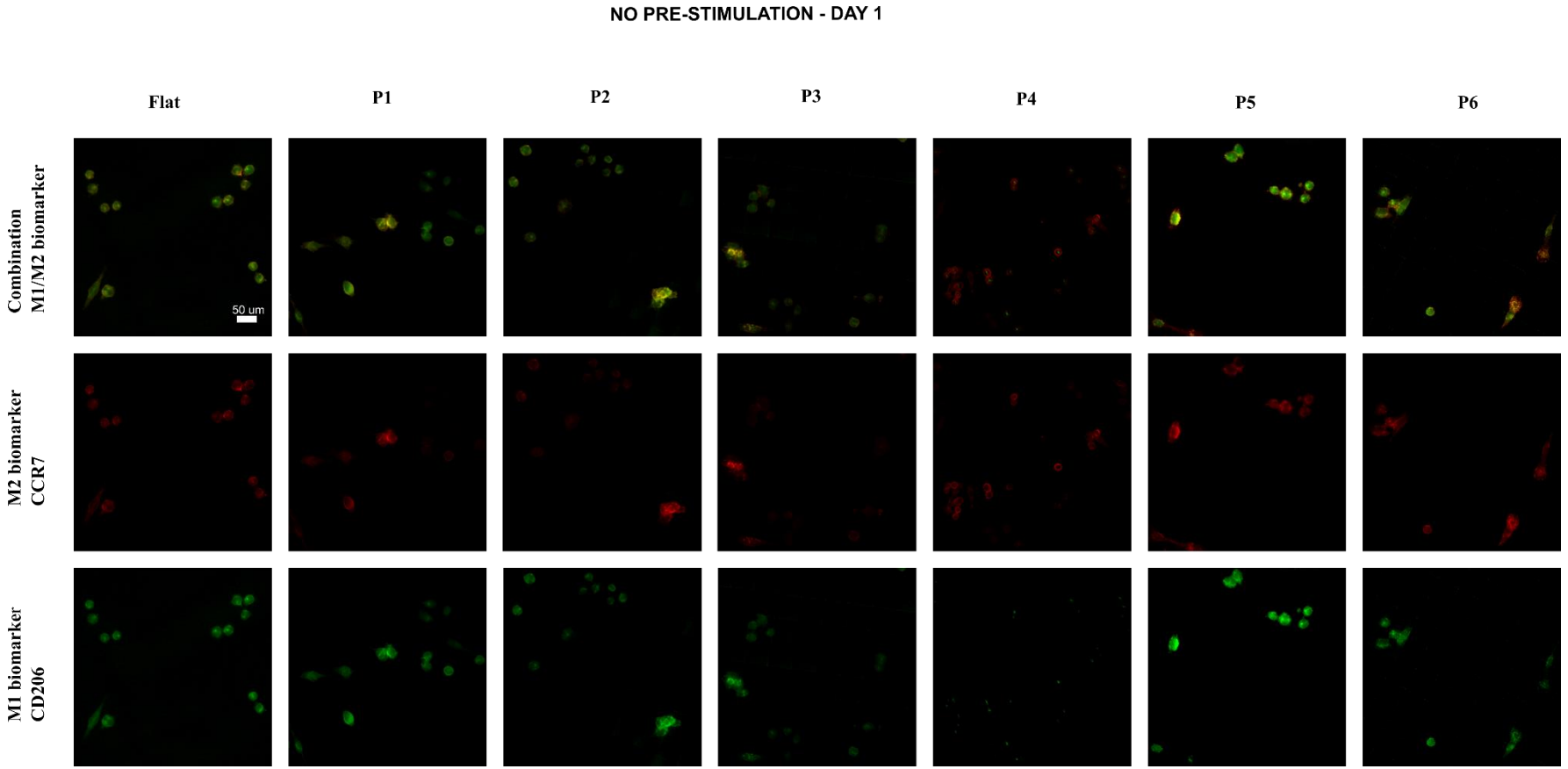

Figure 24: Immunofluorescent images for CCR7 (M1 phenotype in red) and CD206 (M2 phenotype in green) markers in adherent j774A.1 cells on the investigated samples after one day of seeding without pre-stimulation. The scale bar for all pictures is 50 um.

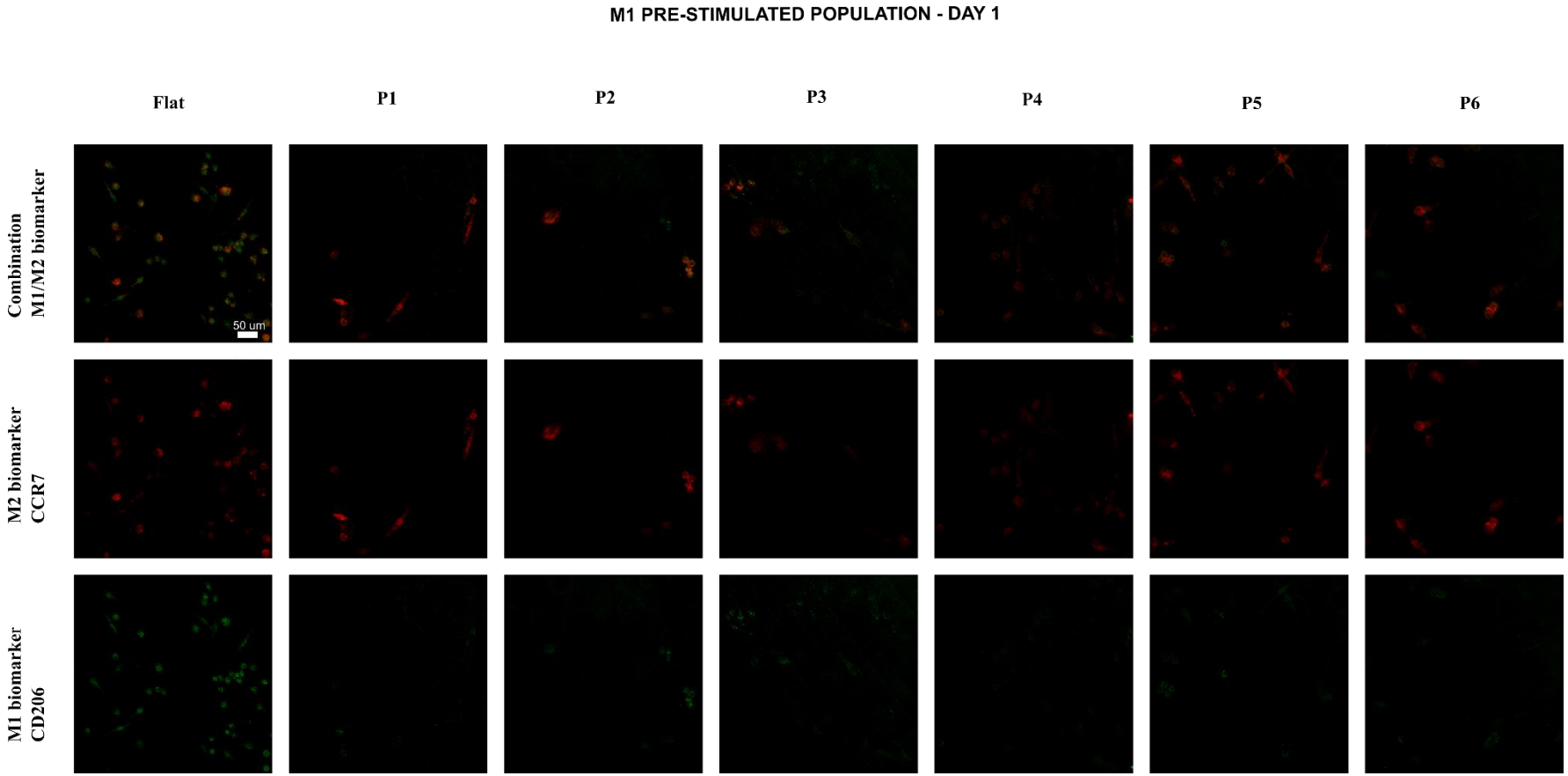

Figure 25: Immunofluorescent images for CCR7 (M1 phenotype in red) and CD206 (M2 phenotype in green) markers in adherent j774A.1 cells on the investigated samples after one day of seeding with pre-stimulation to M1 phenotype. The scale bar for all pictures is 50 um.

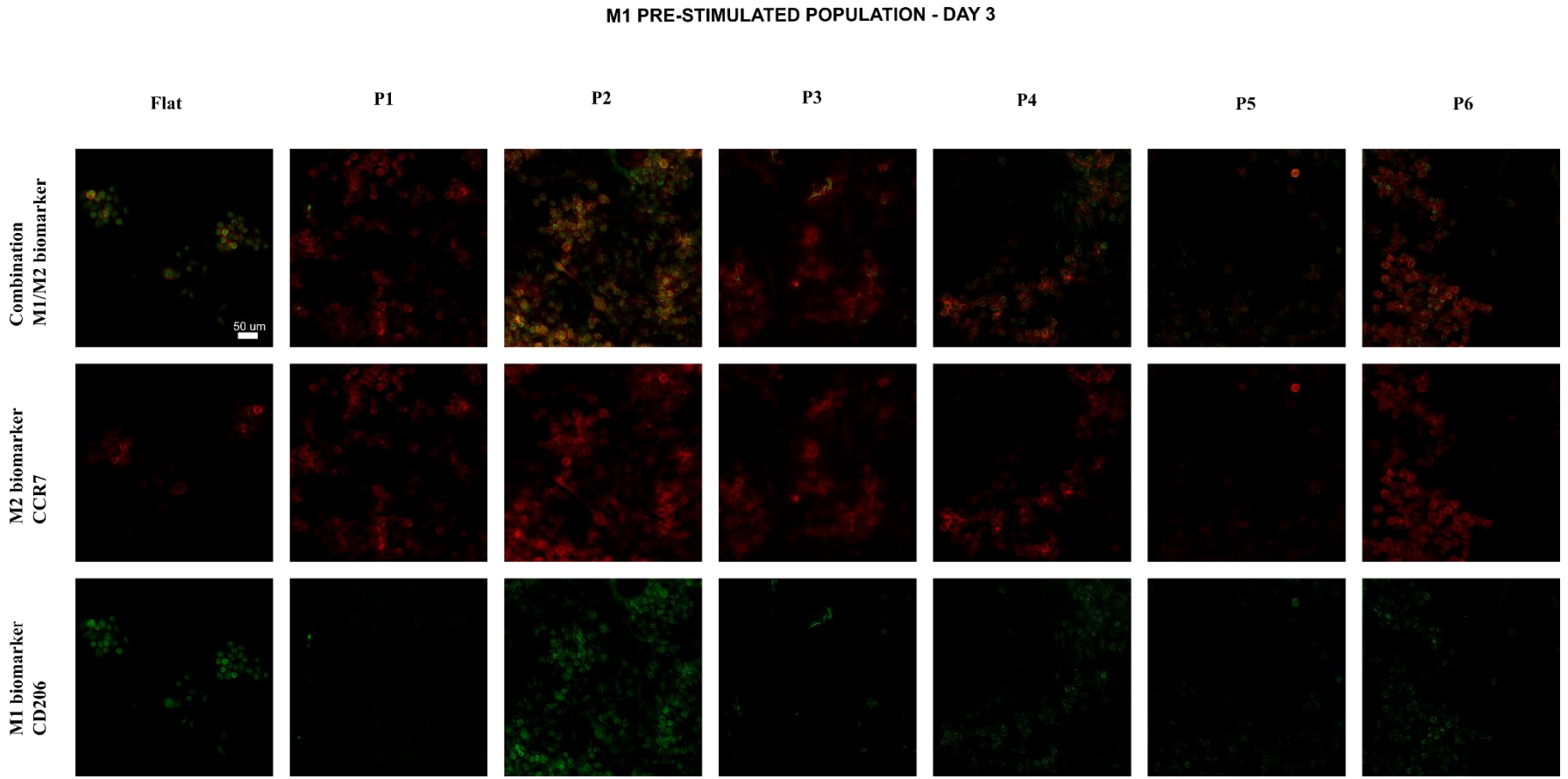

Figure 26: Immunofluorescent images for CCR7 (M1 phenotype in red) and CD206 (M2 phenotype in green) markers in adherent j774A.1 cells on the investigated samples after three days of seeding with pre-stimulation to M1 phenotype. The scale bar for all pictures is 50 um.

Page intentionally left blank

4 Discussion

4.1. Geometrical accuracy of patterns

The geometrical accuracy of the patterns fabricated and used in the project is dependent on and limited by the additive manufacturing technique, the gold-sputtering process, the imaging and the post-processing of the measuring of the acquired images. Additive manufacturing techniques or 3D printing techniques are nowadays widely used in a variety of fields like micro-optics and microelectronics, biomedicine and metamaterials. They have become very sophisticated exceeding farther than simple extrusion of melted plastic and layer-by-layer deposition [37]. The two-photon polymerization process that was used in the context of this project is one of the most novel 3D printing techniques for the fabrication of micro- and nanostructures. The fabrication accuracy of 2PP is the term used to describe the dimensional and shape accuracy as well as the surface roughness. It can be affected by errors of the scanning stage and of the laser beam focus as well as by variance in the preparation and post-processing of the fabricated structure as well as in the environmental conditions. Nanoscribe Photonic Professional GT is known for ultra-precise x-y-z- stage movements attained by its piezoelectric nanopositioning system and for accurate laser beam focus attained by high-precision galvanic mirrors. The photosensitive resist (IP-L780) used for the fabrication of the pillar structures undergoes low shrinkage and is suitable for the fabrication of features down to 160 nm in the x-y direction and up to 450 nm in the z direction with the highest commercially available resolution. One can also argue that 2PP fabrication accuracy is also limited to errors produced because of the CAD file conversion to the .STL file. The laboratory conditions together with pre- and post-processing handling protocols of the fabricated structures can impact their quality and reproducibility to a great extent. UV-exposure of the used photosensitive resist, non-controllable humidity levels and the presence of dust in the laboratory, together with longer exposure times of the fabricated structures to solvents can compromise their quality and result in reduced reproducibility. The resulting thickness of the conductive gold film, during gold-sputtering, is approximately 5 nm for 1 min of gold sputtering at a working distance of 20 mm [38]. Therefore, the geometry of the pillar structures must have been approximately 3.3 nm larger both lateral and vertical direction. Lastly, image acquisition and image processing can result in measurement errors of the pillars' geometry. Therefore, the variance shown in section 3.1.2 is expected and the geometrical accuracy of the patterns can be considered acceptable based on the fact that it did not appear to be statistically significant.

4.2. Submicron pillars support macrophage attachment and affect cell morphology

The effect of 6 different pillar patterns on macrophages' attachment and morphology was investigated in the current study. The number of the cells attached on the patterns were counted and compared across substrates after one day of seeding. The results did not yield a concrete trend describing macrophages' "preference" to a specific pillar height and pitch. More macrophages were found on pattern P2, thus the pillar array with a pillar height of 500 nm and a pillar pitch of 700 nm seemed to be the most preferable one. The macrophages used in this experiment were exhibiting a mixed morphology of round and elongated cells already at pre-culture. According to literature, a round cell morphology indicates a state of inactivity compared to the elongated morphology or a morphology exhibiting fine cytoplasmic extensions [39]. After seeding on the patterns for one day, macrophages' morphology was already affected by the different patterns. It is very interesting that, the morphologically round cells grew larger on the less dense pillar patterns (P4, P5, P6), thus, on the patterns with a pitch of 1000 nm, whereas

the higher and denser the pillar pattern was, the larger in both elongation and size (area) the elongated morphology of the cells. Both morphologies were found on all patterns after one day of seeding and the number of the elongated cells increased with increasing pillar height and pillar pitch of 700 nm. Macrophages also exhibited random alignment on the patterns and this result is in-line with studies on pillar patterns of the same scale [40]. Lastly, pillar detachment on patterns with pillar heights larger than 500 nm was observed whereas no pillar detachment was observed on pillars of 300 nm height, nor any filopodial extensions developing on them. Macrophages' elasticity is shown to be related to the stiffness of the substrate, showing an increasing trend with increasing substrate rigidity [41]. Pillar detachment might therefore be the result of an increase in macrophages' elasticity on pillars larger than 300 nm than surpasses the attachment forces between the pillars and the glass substrate.

4.3. Localization, expression and quantification of phenotypic biomarkers

Dual-fluorescent staining for macrophages with and without prior stimulation after one and three days of seeding showed colocalization of the phenotype markers CD206 (M2) and CCR7 (M1). That indicates a mixed macrophage population comprised from transitory macrophage phenotypes [42]. At the earliest timepoint (day 1), the M1 biomarker is more expressed compared to the M2 biomarker for all patterned substrates, but P4, in the non-stimulated group. For the M1-stimulated group at day 1, the M1 biomarker is less expressed on patterns with the lowest pillar height (P1 and P4), whereas the M2 biomarker shows a significantly higher expression on the pattern with a pillar pitch and height of 1000 nm (pattern P6). For the same groups, that the latest timepoint (day 3), it is becoming evident that some patterns have a greater effect on the M1 to M2 switch than others, with P6 having a greater effect towards the M2 phenotype switch compared to any other substrate including the flat surface. P3 induced much lower levels of M2-switch compared to P6, showing that pillar height is not the only factor influencing phenotype polarization, and that pillar pitch can greatly affect the M1/M2 polarization.

The quantification of the intensity levels of the fluorescent dyes that was employed in the context of the current project was limited by a variety of factors. The image acquisition conditions is the first and most important one because of the variations in the pillar height and pitch that require different image processing settings that result in loss of information. Moreover, in the existing literature immunofluorescent staining is rarely quantifiable and most of the conclusions are drawn by qualitative observation of the pictures. However, this is by far the least reliable method to access and identify differences in the biomarkers' expression. For this specific reason, most of the research on M1 and M2 macrophages is based on alternative biological assays for the quantification of the levels of the corresponding biomarkers, such as ELISA and Western blotting assays. The particularity of the samples however, would not allow the employment of such assays in the context of the current project, and more specifically, it would be impossible to measure, compare and contrast levels of protein expression on samples that are not as a whole patterned but only partially (only 0.25 mm^2 of 706.5 mm^2). Another limitation is the number of cells per sample that could be quantified, and these were only single cells, in order to avoid assumptions of higher M1 or M2 expression because of protein accumulation of overlapping and clustered cells. The coefficient of variation (CV) was calculated for each experimental group and subject and it showed great variability for the majority of the cases. The results of the calculation are presented in Appendix G. Resolution of this problem could be achieved by repeating the experiment. This could also be beneficial to check how the within- and between- sample variation is affected to also determine the optimal replicate number for validation and increase statistical reliability.

Page intentionally left blank

Page intentionally left blank

5 Conclusion

This is the first time that macrophage attachment, morphology and phenotypic changes induced by pillar arrays of different pillar height and pitch were studied in a systematic way *in vitro*. Driven by the advances in the nanofabrication technology the Nanoscribe's Photonic Professional GT laser lithography system was used to repeatedly obtain high-resolution pillar arrays of controlled geometrical characteristics (diameter, height, pitch) and investigate their effect on the J774A.1 macrophages. It was demonstrated that different pillar heights and pillar pitches induce different cell attachment mechanisms and directly affect the size and shape of the macrophages after one day of seeding. Patterns with a height of 1000 nm and a pitch of 700 nm induced an increase in the number of elongated cells. Round cells were showing larger areas when adherent on patterns with a pitch of 1000 nm. Elongated macrophages were strongly affected by patterns of 1000 nm height and 700 nm pitch. Moreover, after one day of seeding, non-stimulated macrophages on patterns expressed a pro-inflammatory M1 phenotype compared to the macrophage seeded on the flat control substrate that clearly express a pro-healing M2 phenotype. M1 stimulated macrophages on patterns with a pillar height and pitch of 1000 nm were greatly affected with regards to their phenotype, showing stronger M2 expression already after one day of seeding. After 3 days of seeding these exact geometrical characteristics are shown to be the more potent leading to a M1/M2 macrophage phenotype switch. In the frame of the current project, it was demonstrated that the patterns fabricated are cytocompatible, affect cell morphology and are also immunomodulatory.

6 Suggestions for future research

Regarding the limitations of the current research, as they were presented so far, some suggestions that could validate and consolidate the knowledge obtained include the following points listed in a relative priority order:

1. Validation of the CD206/CCR7 results could be achieved by repeating the experiment more times for the groups that show higher CV values. Alternatively, single fluorescent staining for the phenotype could also validate the results.
2. Only the effect of pillars on M1-stimulated and non-stimulated cells was investigated in this project. Another way to validate the immunomodulatory profile of the pillars could also be to start off with M2-stimulated macrophages to seed on the pillars.
3. The 2PP fabrication process requires very delicate pre- and post-fabrication handling of the samples, as well as, very controlled laboratory conditions to achieve reproducibility of the results. Moreover, it is a relatively slow fabrication process regarding the patterned area. Nanoimprint lithography could be considered as an alternative fabrication process to fabricate larger areas of pillar array in a shorter fabrication time.
4. Since pillar detachment took place already after one day of seeding, it would be beneficial to fabricate stiffer pillar arrays and repeat both the experiment about the morphology and the phenotype to detect differences. For deeper understanding of the cytoskeletal re-organization and how this affects the cellular response of macrophages, focal adhesion staining with vinculin could be employed and imaging could be performed with a confocal microscope.

5. The J774A.1 macrophages seeded on the patterns exhibited morphological differences, thus they were comprised by a mixed population of round and elongated cells since the pre-seeding step. It could be interesting to monitor their proliferation for longer periods also combined with different cell culture medium like RPMI 1640.
6. M1 and M2 macrophage phenotypes can be identified by a variety of biomarkers employing a variety of biological assays. In the current project only 4 of them were used (ARG-1, iNOS, CCR7, CD206) by means of fluorescent staining. More biomarkers could be tried using assays that combine simultaneous detection of multiple biomarkers (e.g. ELISA assay) for broader understanding of the macrophage polarization mechanism.
7. In the current project, macrophage polarization was evaluated at two timepoints, however, monitoring the process for longer periods using live cell imaging techniques could enable the collection of solid evidence about the cellular dynamics that develop between the pillar patterns and the macrophages.

References

[1] N. Huebsch and D. J. Mooney, "Inspiration and application in the evolution of biomaterials," *Nature*, vol. 462, 2009.

[2] C. P. Newswire. (2019) Global Orthopedic Device Market Growth. Available: https://www.prnewswire.com/news-releases/global-orthopedic-device-market-is-anticipated-to-grow-at-a-cagr-of-3-55-from-2019-to-2027-and-reach-us-58-400-million-by-2027--owing-to-cutting-edge-technological-advancements-in-booming-the-orthopedic-market-across-the-globe--300883180.html

[3] J. S. S. *et al.*, "Independent predictors of failure up to 7.5 years after 35 386 single-brand cementless total hip replacements," *The Bone & Joint Journal*, vol. 95-B, 2013.

[4] Z. Chen *et al.*, "Osteoimmunomodulation for the development of advanced bone biomaterials," *Materials Today*, vol. 19, 2016.

[5] J. M. Anderson, "Biological Responses to Materials," *Annual Review of Materials Research*, vol. 31, 2001.

[6] C. M. Champagne, J. Takebe, S. Offenbacher, and L. F. Cooper, "Macrophage cell lines produce osteoinductive signals that include bone morphogenetic protein-2," *Bone*, vol. 30, 2002.

[7] K. Anselme, P. Davidson, A. M. Popa, M. Giazzon, M. Liley, and L. Ploux, "The interaction of cells and bacteria with surfaces structured at the nanometre scale," *Acta Biomaterialia*, vol. 6, 2010.

[8] A. W. Orr, B. P. Helmke, B. R. Blackman, and M. A. Schwartz, "Mechanisms of Mechanotransduction," *Developmental Cell*, vol. 10, 2006.

[9] F. J. Alenghat and D. E. Ingber, "Mechanotransduction: All Signals Point to Cytoskeleton, Matrix, and Integrins", 2002.

[10] J. M. Rice, J. A. Hunt, J. A. Gallagher, P. Hanarp, D. S. Sutherland, and J. Gold, "Quantitative assessment of the response of primary derived human osteoblasts and macrophages to a range of nanotopography surfaces in a single culture model in vitro," (in eng), *Biomaterials*, vol. 24, 2003.

[11] D. Karazisis *et al.*, "The role of well-defined nanotopography of titanium implants on osseointegration: cellular and molecular events in vivo," (in eng), *International journal of nanomedicine*, vol. 11, 2016.

[12] D. Karazisis *et al.*, "The influence of controlled surface nanotopography on the early biological events of osseointegration," (in eng), *Acta Biomater*, vol. 53, 2017.

[13] M. Mohiuddin, H. A. Pan, Y. C. Hung, and G. S. Huang, "Control of growth and inflammatory response of macrophages and foam cells with nanotopography," (in eng), *Nanoscale Res Lett*, vol. 7, 2012.

[14] S. Zhang *et al.*, "Polylactic Acid Nanopillar Array-Driven Osteogenic Differentiation of Human Adipose-Derived Stem Cells Determined by Pillar Diameter," (in eng), *Nano Lett*, vol. 18, 2018.

[15] H. Cao, K. Mchugh, S. Y. Chew, and J. M. Anderson, "The topographical effect of electrospun nanofibrous scaffolds on the in vivo and in vitro foreign body reaction," *Journal of Biomedical Materials Research Part A: An Official Journal of The Society for Biomaterials, The Japanese Society for Biomaterials, and The Australian Society for Biomaterials and the Korean Society for Biomaterials*, vol. 93, 2010.

[16] E. Saino *et al.*, "Effect of electrospun fiber diameter and alignment on macrophage activation and secretion of proinflammatory cytokines and chemokines," (in eng), *Biomacromolecules,* vol. 12, 2011.
[17] K. Wang *et al.*, "Overcoming foreign-body reaction through nanotopography: Biocompatibility and immunoisolation properties of a nanofibrous membrane," (in eng), *Biomaterials,* vol. 102, 2016.
[18] S. Chen, J. A. Jones, Y. Xu, H.-Y. Low, J. M. Anderson, and K. W. Leong, "Characterization of topographical effects on macrophage behavior in a foreign body response model," *Biomaterials,* vol. 31, 2010.
[19] J. Y. Kim, D. Khang, J. E. Lee, and T. J. Webster, "Decreased macrophage density on carbon nanotube patterns on polycarbonate urethane," *Journal of Biomedical Materials Research Part A,* vol. 88A, 2009.
[20] E. Lamers *et al.*, "In vitro and in vivo evaluation of the inflammatory response to nanoscale grooved substrates," (in eng), *Nanomedicine : nanotechnology, biology, and medicine,* vol. 8, 2012.
[21] X. Li *et al.*, "Effects of titanium surface roughness on the mediation of osteogenesis via modulating the immune response of macrophages," (in eng), *Biomed Mater,* vol. 13, 2018.
[22] T. U. Luu, S. C. Gott, B. W. Woo, M. P. Rao, and W. F. Liu, "Micro- and Nanopatterned Topographical Cues for Regulating Macrophage Cell Shape and Phenotype," (in eng), *ACS Appl Mater Interfaces,* vol. 7, 2015.
[23] H. Pan *et al.*, "Immunomodulation effect of a hierarchical macropore/nanosurface on osteogenesis and angiogenesis," (in eng), *Biomed Mater,* vol. 12, 2017.
[24] M. Nouri-Goushki *et al.*, "Submicron patterns-on-a-chip: Fabrication of a microfluidic device incorporating 3D printed surface ornaments," *ACS Biomaterials Science & Engineering,* vol. 5, 2019.
[25] W. S. Rasband. (1997-2018). *ImageJ*, National Institutes of Health, Bethesda, Maryland, USA. [Online]. Available: https://imagej.nih.gov/ij/.
[26] "Chapter 5 - Laboratory Diagnosis of Viral Infections," in *Fenner's Veterinary Virology (Fifth Edition)*, N. J. MacLachlan and E. J. Dubovi, Eds. Boston: Academic Press, 2017.
[27] T. Scientific. (02/11/2019). *Immunolabeling* [Online]. Available: https://www.thermofisher.com/nl/en/home/life-science/cell-analysis/cell-analysis-learning-center/molecular-probes-school-of-fluorescence/imaging-basics/labeling-your-samples/immunolabeling.html.
[28] N. C. f. B. Information, "Arginine, CID=6322," in *PubChem Database*, ed.
[29] Y. C. Luiking and N. E. P. Deutz, "Biomarkers of Arginine and Lysine Excess," *The Journal of Nutrition,* vol. 137, 2007.
[30] R. B. Caldwell, H. A. Toque, S. P. Narayanan, and R. W. Caldwell, "Arginase: an old enzyme with new tricks," (in eng), *Trends Pharmacol Sci,* vol. 36, 2015.
[31] U. Schultz and K. E. Magor, "Chapter 21 - Comparative Immunology of Agricultural Birds," in *Avian Immunology (Second Edition)*, K. A. Schat, B. Kaspers, and P. Kaiser, Eds. Boston: Academic Press, 2014.
[32] A. K. Azad, M. V. S. Rajaram, and L. S. Schlesinger, "Exploitation of the Macrophage Mannose Receptor (CD206) in Infectious Disease Diagnostics and Therapeutics," (in eng), *J Cytol Mol Biol,* vol. 1, 2014.
[33] K. A. Jablonski *et al.*, "Novel Markers to Delineate Murine M1 and M2 Macrophages," (in eng), *PloS one,* vol. 10, 2015.

[34] N. Fahy *et al.*, "Human osteoarthritic synovium impacts chondrogenic differentiation of mesenchymal stem cells via macrophage polarisation state," *Osteoarthritis and Cartilage*, vol. 22, 2014.
[35] Wikipedia. (2019). *Griess Test* [Online]. Available: https://en.wikipedia.org/wiki/Griess_test.
[36] G. Wypych, "1 - PHOTOPHYSICS," in *Handbook of Material Weathering (Sixth Edition)*, G. Wypych, Ed.: ChemTec Publishing, 2018.
[37] X. Zhou, Y. Hou, and J. Lin, "A review on the processing accuracy of two-photon polymerization," *AIP Advances*, vol. 5, 2015.
[38] JEOL. *JEOL JFC-1300 AUTO Sputter Coater* [Online]. Available: https://www.jeolusa.com/PRODUCTS/Sample-Preparation-Tools/Smart-Coater.
[39] F. Heinrich *et al.*, "Morphologic, phenotypic, and transcriptomic characterization of classically and alternatively activated canine blood-derived macrophages in vitro," (in eng), *PLoS One*, vol. 12, 2017.
[40] J. Padmanabhan *et al.*, "Engineering Cellular Response Using Nanopatterned Bulk Metallic Glass," *ACS Nano*, vol. 8, 2014.
[41] N. R. Patel *et al.*, "Cell Elasticity Determines Macrophage Function," *PLoS One*, vol. 7, 2012.
[42] K. R. Nakazawa *et al.*, "Accumulation and localization of macrophage phenotypes with human intervertebral disc degeneration," (in eng), *Spine J*, vol. 18, 2018.

List of tables

List of figures

Appendices

A. Pattern designs

A.1 Pillar pattern with random pillar heights and constant pillar pitch

Python script

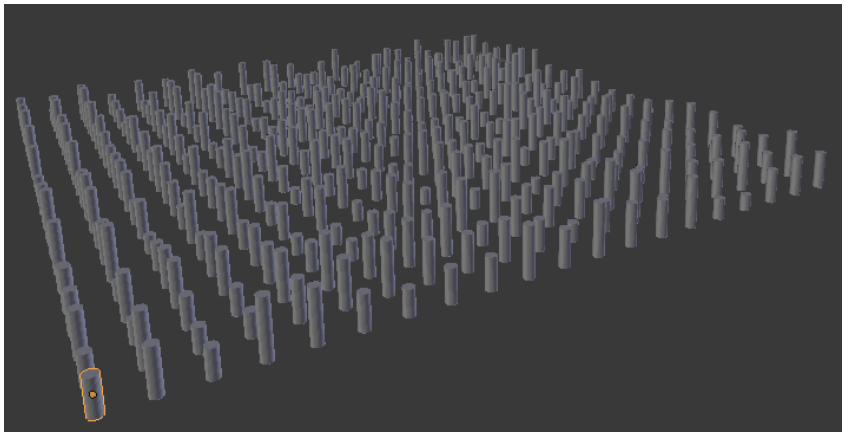

```
import bpy, random
from math import radians
from mathutils import Vector

row = 20
column = 20

for i in range(row):
    for j in range(column):
        l = Vector()
        r = Vector()
        d = Vector()
        l.x = i*7
        l.y = j*7
        d=random.uniform(3,10)
        l.z = d/2
        for xyz in r:
            r.xyz = radians(0)
        bpy.ops.mesh.primitive_cylinder_add(vertices=36,
                                            radius=1,
                                            depth=d,
                                            location=l,
                                            rotation=r,
                                            )
```

A.2 Pillar pattern with gradient pillar height and constant pillar pitch

Python script

```
import bpy, import bmesh
import math
from mathutils import Vector

RADIUS = 0.16
HEIGHT = 32
SEGMENTS = 32
DISTANCE = 1
COLS = 20
ROWS = 20
SCALE = 1
MEAN = 0
STD_DEVIATION = 4

def normal_dist(x):
    global MEAN, STD_DEVIATION
    mean = MEAN
    std_deviation = STD_DEVIATION

    exponent = - math.pow(x - mean, 2) / (2 * math.pow(std_deviation, 2))
```

```
    return 1 / (std_deviation  * math.pow(2*math.pi,  0.5)) * math.exp(exponent)

bm = bmesh.new()
bmesh.ops.create_circle(bm,  segments=SEGMENTS,  diameter=RADIUS*2,  cap_ends=True)
bm.faces.ensure_lookup_table()
ret = bmesh.ops.extrude_discrete_faces(bm,  faces=bm.faces)
bmesh.ops.translate(bm,  vec=Vector((0,0,  HEIGHT)),  verts=ret['faces'][0].verts)

 scn = bpy.context.scene

name = "me"

for i in range(COLS):
    for j in range(ROWS):
        pos = Vector((i - COLS/2, j - COLS/2, 0))
        pos *= DISTANCE

        name = "cylinder_" + str(i) + "_" + str(j)
        if name not in bpy.data.meshes:
            me = bpy.data.meshes.new(name)
        else:
            me = bpy.data.meshes[name]
        bm.to_mesh(me)

        if name not in bpy.data.objects:
            ob = bpy.data.objects.new(name,  me)
        else:
            ob = bpy.data.objects[name]
            ob.data = me

        ob.location = pos.copy()
        pos *= SCALE
        ob.scale.z = normal_dist(pos.x) * normal_dist(pos.y)  * HEIGHT

        if ob.name  not in scn.objects:
            scn.objects.link(ob)


bm.free()
```

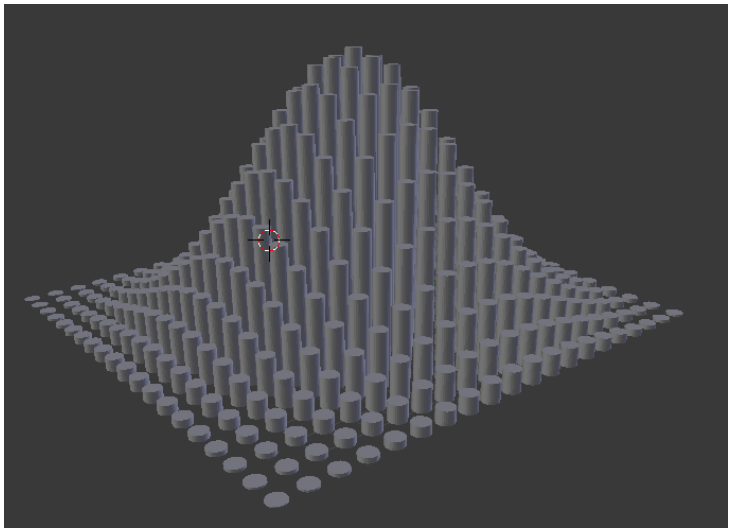

B. Handling protocols for J774A.1 cell line

B.1 Cell seeding pre-culture Protocol for J774A.1 macrophages

Equipment

1.5 ml tubes
50 ml tubes
P20 pipette + filter tips
P1000 pipette + filter tips
5ml plastic pipettes
10ml plastic pipettes
75 cm^2 flask
Suction system
Water bath at 37 °C
50 ml tube centrifuge

Reagents

DMEM

Cells

1 vial of frozen J774A.1 cells (1ml)

Procedure

1. Fill one 50 ml with 10 ml of pre-warmed DMEM.
2. Take a vial from the -80 °C and directly put the vial in the water bath, watch the vial closely until any ice has melted. Hold the vial and not just put it as a whole in the water bath.
3. Write down the passage number written in the vial and wipe the vial with ethanol before placing it in the biosafety cabinet.
4. Pipette the cells with the P1000 pipette into the 50 ml tube. Rinse the vial twice with 1ml DMEM and add to the same 50 ml tube.
5. Adjust the DMEM volume to 25 ml.
6. Spin-down for 5 mins at 200x g (you can see the cells forming a clump at the bottom of the 50 ml tube).
7. Remove the supernatant carefully using the suction system.
8. Resuspend the cells in 1ml of DMEM pipetting up and down with the P1000 until no clumps of cells are visible anymore.
9. Transfer 2 samples of 10 µL each into 1.5 ml tubes to count the amount of cells.
10. Seed approximately 5 x 10^5 cells per 75 cm^2 flask in 10 ml DMEM.
11. Distribute the cells by carefully shaking the flask.
12. Transfer the flask to the CO_2 incubator (37°C, 5% CO_2).
13. Refresh the DMEM every 2 to 3 days.
14. Use the cells when they are confluent.

B.2 Cell seeding for experiment Protocol for J774A.1 macrophages

Equipment

1.5 ml tubes
50 ml tubes
P20 pipette + filter tips
P1000 pipette + filter tips
5ml plastic pipettes
10ml plastic pipettes
Cell scraper
75 cm^2 flask
Suction system
Water bath at 37 °C
50 ml tube centrifuge

Reagents

DMEM

Cells

Pre-cultured J774A.1 cells

Procedure

1. Remove some of the DMEM from the flask using a 10 ml pipette and the suction system (Make sure some DMEM stays in the flask ~10 ml).
2. Use the cell scraper to detach the cells from the flask bottom. Move the cell scraper crosswise (from one slide to the other of the flask) a couple of times.
3. Check whether the cells have detached in the microscope. If there are still attached cells repeat step 2.
4. Pipette the cells with the 10 ml pipette into the 50 ml tube. Rinse the flask with another 10 ml of DMEM and add to the same 50 ml tube.
5. Adjust the DMEM volume to 25 ml.
6. Spin-down for 5 mins at 200x g (you can see the cells forming a clump at the bottom of the 50 ml tube).
7. Remove the supernatant carefully using the suction system.
8. Resuspend the cells in 1ml of DMEM pipetting up and down with the P1000 until no clumps of cells are visible anymore.
9. Transfer 2 samples of 10 µL each into 1.5 ml tubes to count the amount of cells.
10. Seed the appropriate amount of cells, depending on the experiment (Add 2ml of DMEM to the wells and seed 50.000 cells/well).
11. Distribute the cells evenly by carefully shaking the plate.
12. Incubate the plate in the CO_2 incubator (37°C, 5% CO_2).

B.3 Live/Dead Staining Protocol for J774A.1 macrophages

Equipment

P2 pipette + filter tips
P20 pipette + filter tips
P1000 pipette + filter tips
1.5 ml tubes
Fluorescent microscope

Reagents

LIVE/DEAD™ Viability/Cytotoxicity Kit, for Mammalian Cells (#L3224 ThermoFisher Scientific, US)

Cells

Pre cultured well plate

Procedure

1. Pre culture cells for 2 days
2. Wash the cells with 10x PBS
3. Wash the cells with 1x PBS
4. Prepare Live/dead solution in 1ml 1xPBS, Calcein AM: 0.1µl, EthD-1: 1.5µl
5. Incubate sample for 30 minutes.
6. Discard solution and replace with 1x PBS.
7. Image by fluorescent microscope

Live cells: bright green signal
Dead cells: red + green signal

B.4 Phenotype Staining Protocol for J774A.1 macrophages

Equipment

P1000 pipette + filter tips
Disposable pipettes (BRAND pipette, Sigma Aldrich # Z331676)
6x well plates (Greiner Bio- one # 657160)
Microscope glass slides

Reagents

DPBS (#14200083, ThermoFisher Scientific, US)
Formaldehyde (Sigma-Aldrich 252549)
Blocking Reagent (UltraCruz, Santa Cruz, sc-516214, US)
Triton (Sigma-Aldrich # T8787-250ml)
Tween (Sigma-Aldrich # P1379-100ml)
NOS2 Antibody (C-11) (Santa Cruz, sc-7271, US)
Anti-liver Arginase antibody rabbit anti-mouse (ab91279, Abcam, UK)
Anti-Mannose Receptor antibody - CD206 (ab8918, Abcam, UK)
Recombinant Anti-CCR7 antibody (ab32527, Abcam, UK)
Alexa-Fluor 488 donkey anti-mouse (#10544773,ThermoFisher Scientific, US)
Alexa-Fluor 594 donkey anti-rabbit (#10798994, ThermoFisher Scientific, US)
Prolong glue (Invitrogen # P36931)

Cells

Precultured cells on a glass slide

Procedure

1. Wash the cells twice with DPBS.
2. Transfer the cells to the chemical hood.
3. Add 2ml of 4% formaldehyde solution to the cells.
4. Incubate for 15 mins at room temperature.
5. Discard the formaldehyde solution.
6. Wash the cells twice with DPBS.
7. Permeabilize the cells with 0.5% Triton/DPBS solution for 15 mins at 4 °C.
8. Discard the Triton solution.
9. Add the blocking Santa Cruz solution and incubate at 37 °C for 5 mins.
10. Dilute the primary antibody for iNOS (1:100) and ARG-1 (1:100) in the blocking Santa Cruz solution and incubate overnight at 4 °C.
11. Wash with Tween 3 times and 5 mins at room temperature.
12. Dilute the secondary antibodies Alexa-Fluor 488 (1:100) and Alexa-Fluor 594 (1:100) and incubate for 1 hour at room temperature.
13. Wash the cells with DPBS for 5 mins at room temperature.
14. Mount glass slide on a microscope slide with glue (containing DAPI) to object glass.

Note: for staining with CD206/CCR7 follow the above procedure only changing the blocking and diluting medium to 1% BSA/PBS instead of using UltraCruz. Dilution concentrations for primary antibodies are 1:100 and for Alexa-Fluor 488 1:50 and Alexa-Fluor 594 1:150.

B.5 Cytoskeleton Staining Protocol for J774A.1 macrophages

Equipment

P1000 pipette + filter tips
Disposable pipettes
6x well plates
Microscope glass slides

Reagents

DPBS (#14200083,ThermoFisher Scientific, US)
Formaldehyde (Sigma-Aldrich 252549)
Blocking Reagent (UltraCruz, Santa Cruz, sc-516214, UK)
Triton (Sigma-Aldrich # T8787-250ml)
Tween (Sigma-Aldrich # P1379-100ml)
Rhodamine- phalloidin (#10063052, ThermoFisher Scientific, US)
Alexa-Fluor 488 donkey anti-mouse (#10544773, ThermoFisher Scientific, US)
Prolong glue (Invitrogen # P36931)

Cells

Precultured cells on a glass slide

Procedure

1. Wash the cells twice with DPBS.
2. Transfer the cells to the chemical hood.
3. Add 2ml of 4% formaldehyde solution to the cells.
4. Incubate for 15 mins at room temperature.
5. Discard the formaldehyde solution.
6. Wash the cells twice with DPBS.
7. Permeabilize the cells with 0.5% Triton/DPBS solution for 15 mins at 4 °C.
8. Discard the Triton solution.
9. Add 1% BSA/PBS and incubate at 37 °C for 5 mins.
10. Dilute the primary antibody for rhodamine-phalloidin (0.1:100) in 1% BSA/PBS and incubate for 1 hour at 37 °C.
11. Wash with 0.5% Tween/PBS 3 times and 5 mins at room temperature.
12. Dilute the secondary antibody Alexa-Fluor 488 (1:100) in 1% BSA/PBS and incubate for 1 hour at room temperature.
13. Wash cells with 0.5% Tween/PBS 3 times 5 minutes at room temperature.
14. Wash the cells with DPBS 3 mins and 5 mins at room temperature.
15. Mount glass slide on a microscope slide with glue (containing DAPI) to object glass.

B.6 Dehydration process of samples

Equipment
Pipettes

Reagents
Ethanol 96%
Ethanol 70%
Ethanol 50%
Distilled water

Cells
Precultured J774A.1 cells on samples

Procedure
1. Remove the fixative by washing the samples with distilled water twice for 5 mins.
2. Discard the distilled water and add ethanol 50% to the samples. Incubate for 15 mins.
3. Discard ethanol 50% and add ethanol 70% to the samples. Incubate for 20 mins.
4. Discard ethanol 70% and add ethanol 96% to the samples. Incubate for 20 mins.
5. Discard ethanol 96% and let the sample dry for at least 2 hours or overnight in the chemical hood.
6. Mount the samples on the sample holder and image at the SEM.

B.7 LPS Stimulation Protocol for J774A.1 macrophages

Equipment
6x well plates
50ml tubes
Pipettes

Reagents
DPBS
DMEM LPS

Cells
Precultured J774A.1 cells

Procedure
1. Make a solution of DMEM, LPS and INF-γ with an LPS concentration of 100ng/ml and an INF-γ concentration of 10ng/ml.
2. Seed the cell at the appropriate cell density on the glass slides in a 6-well plate using the LPS/INF-γ-solution as the cell culture medium.
3. Incubate at 37°C for 72h.
4. Discard the cell culture medium.
5. Wash with DPBS twice.
6. Proceed with the phenotype staining protocol.

B.8 IL-4 Stimulation Protocol for J774A.1 macrophages

Equipment

6x well plates
50ml tubes
Pipettes

Reagents

DPBS
DMEM
IL-4

Cells

Precultured J774A.1 cells

Procedure

1. Make a solution of DMEM and IL-4 with an IL-4 concentration of 10 ng/ml.
2. Seed the cell at the appropriate cell density on the glass slides in a 6-well plate using the IL-4-solution as the cell culture medium.
3. Incubate at 37°C for 72h.
4. Discard the cell culture medium.
5. Wash with DPBS twice.
6. Proceed with the phenotype staining protocol.

C. LPS stimulation of J774A.1 – Experimental design and results

LPS concentration	**Stimulation time**	**Cell seeding density**	**Hypothesis and biomarkers**
50ng/ml	24h	50.000 cells/well on 30mm flat glass coverslip	"LPS stimulated cells express more iNOS" iNOS: M1 phenotype marker (green) ARG1: M2 phenotype marker (red)
100ng/ml			
500ng/ml			
1000ng/ml			
50ng/ml	48h		
100ng/ml			
500ng/ml			
1000ng/ml			
50ng/ml	72h		
100ng/ml			
500ng/ml			
1000ng/ml			

LPS 24H STIMULATION

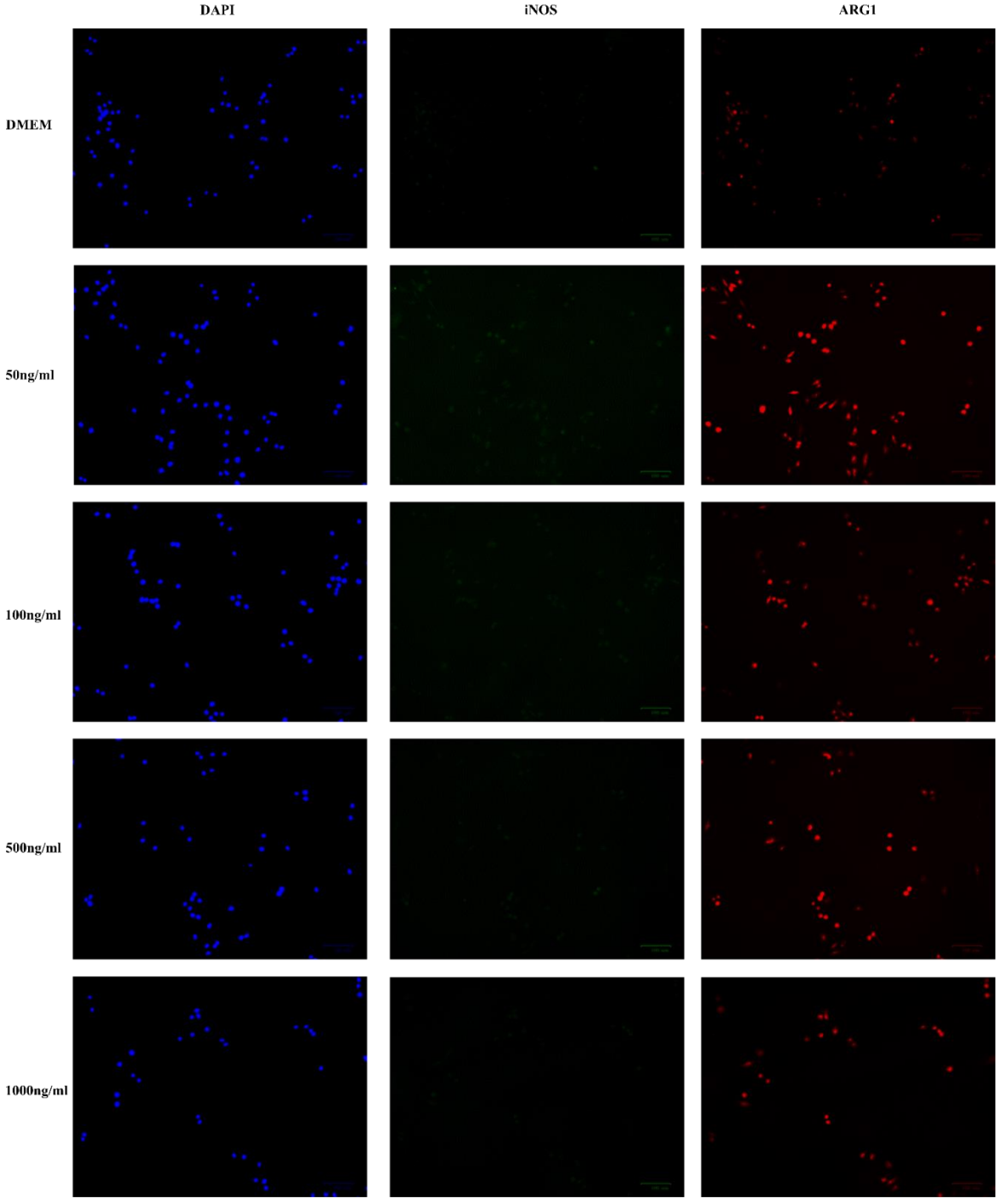

LPS 48H STIMULATION

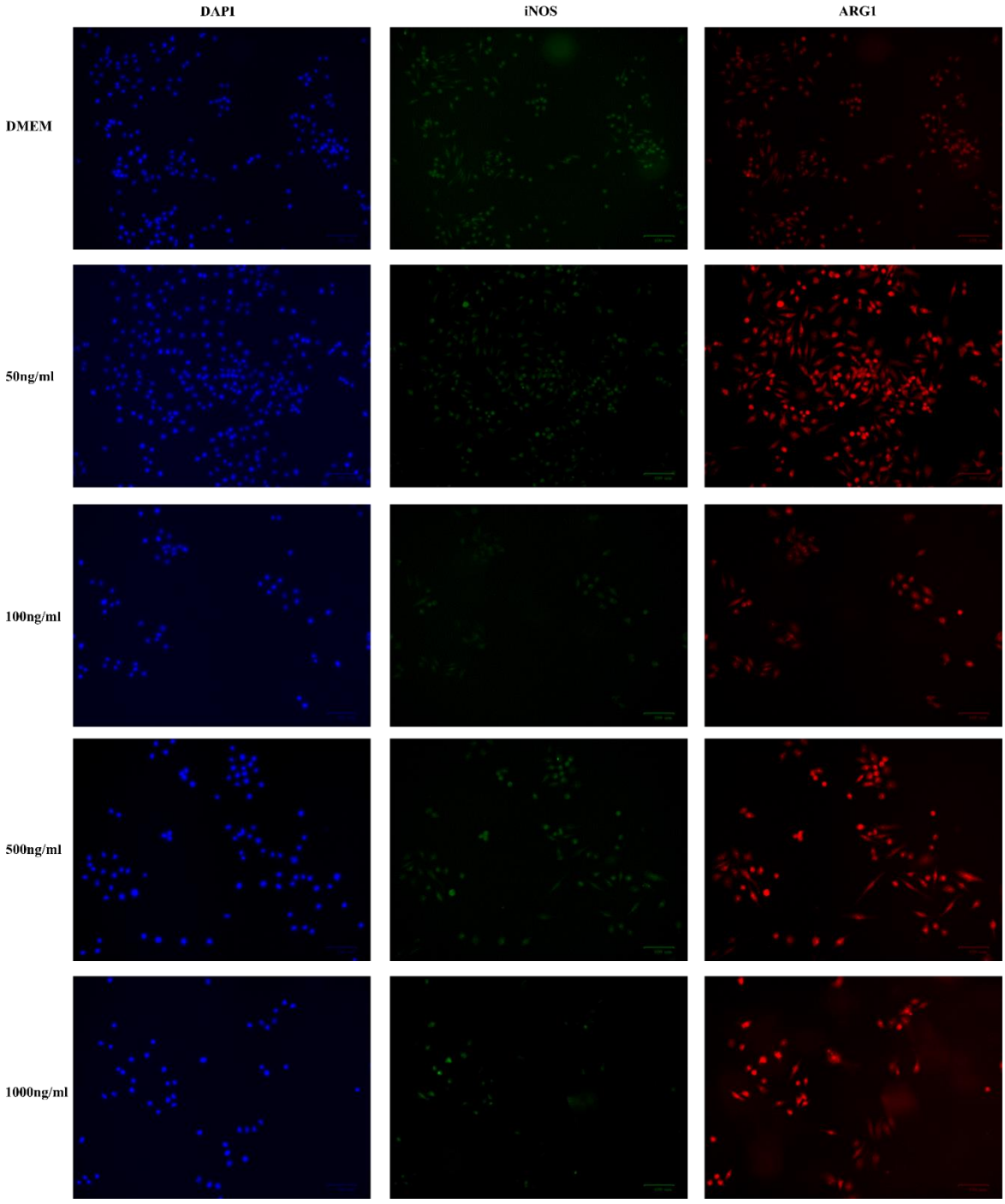

LPS 72H STIMULATION

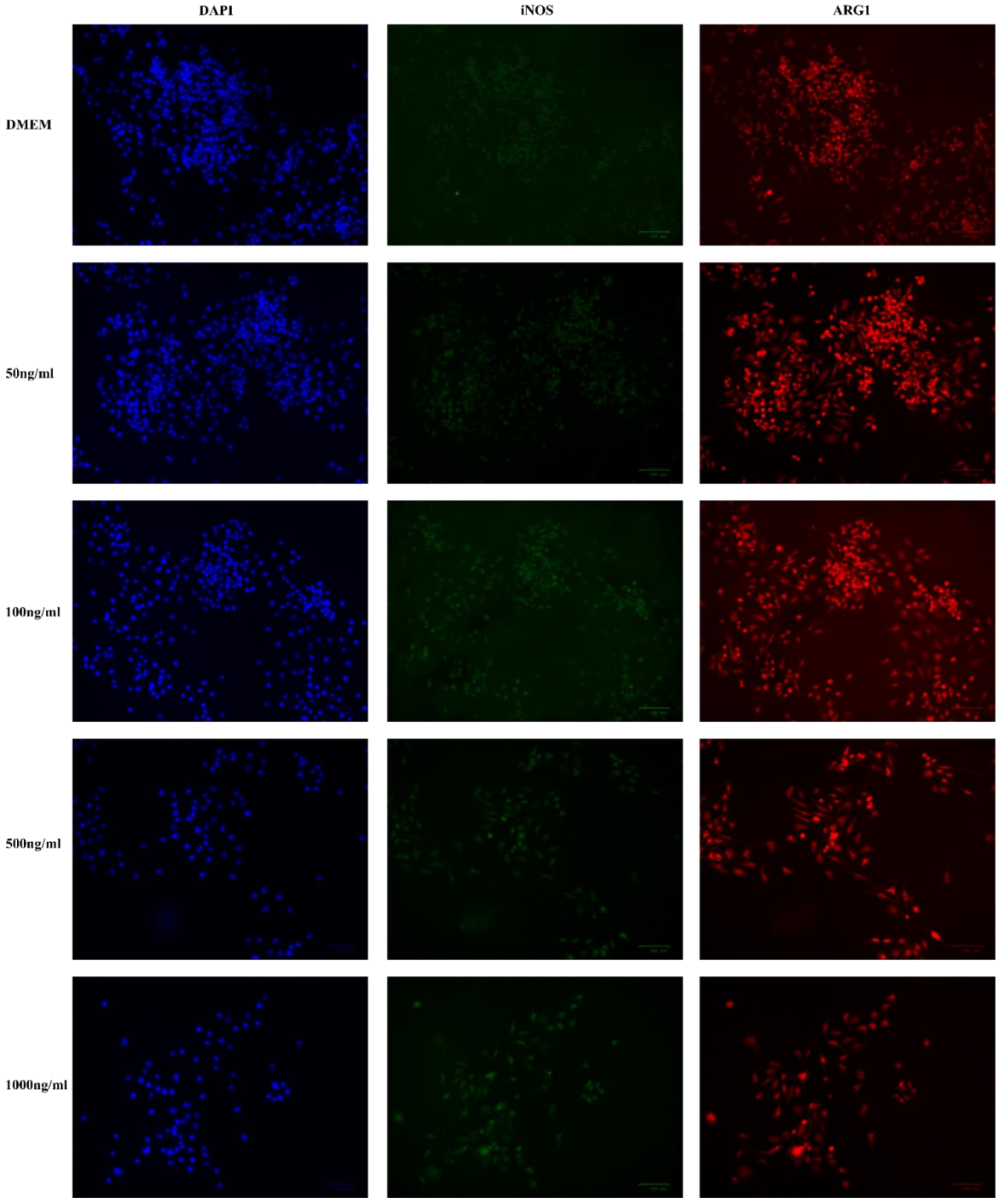

D. Griess assay protocol

D.1 Reagent Preparation

Briefly centrifuge small vials at low speed prior to opening.

Nitrate Assay Buffer: Ready to use as supplied.
Griess Reagent I: Ready to use as supplied.
Griess Reagent II: Ready to use as supplied.
Nitrite Standard: Reconstitute with 100 µL Nitrite Assay Buffer to generate 100 mM Nitrite Standard solution. Keep on ice during use.

D.2 Standard Preparation

Always prepare a fresh set of standards for every use.
Discard working standard dilutions after use as they do not store well.

1. Dilute Nitrite Standard from Step 5.4 100-fold by adding 5 µl of 100 mM Nitrite Standard to 495 µl Nitrite Assay Buffer to obtain 1 mM Nitrite Standard Solution.
2. Using the 1 mM Nitrite Standard Solution, prepare standard curve dilution as described in the table in a microplate or microcentrifuge tubes:

Standard #	1mM Nitrite Standard (µL)	Assay Buffer (µL)	Final volume standard in well (µL)	End amount Nitrite Standard in well (nmol/well)
1	0	200	100	0
2	4	196	100	2
3	8	192	100	4
4	12	188	100	6
5	16	184	100	8
6	20	180	100	10

Each dilution has enough standard to set up duplicate readings (2 x 100 µL).

D.3 Sample Preparation

Collect the cell culture medium and centrifuge it at 1000 x g for 15 mins and transfer the cell supernatant to a new tube.

D.4 Assay Procedure

- Equilibrate all materials and prepared reagents to room temperature just prior to use and gently agitate.
- Assay all standards, controls and samples in duplicate.

<u>Reaction wells set up</u>

Standard wells = 100 µl standard dilutions.
Sample wells = 10-100 µl samples (adjust volume to 100 µl/well with Nitrite Assay Buffer).
Sample Background Control wells = 10-100 µl samples (adjust volume to 100 µl/well with Nitrite Assay Buffer).

<u>Reaction mix:</u>

For each well, add the following reagents in the order indicated in the table below.
Note: Do NOT premix Griess Reagents prior the experiment.

Component Reaction	Mix (µl)	Background Reaction Mix (µl)
Griess Reagent I	10	10
Griess Reagent II	10	--
Nitrite Assay Buffer	80	90

1. Add both Griess Reagents and the Nitrite Assay Buffer separately to each well containing the Standard, Test samples. Mix well.
2. Add 100 µl of Background Reaction Mix into the background control sample wells. Mix well.

Note: For samples exhibiting significant background, it is important prepare parallel sample well(s) as background controls.

D.5 Measurement

1. Incubate the plate for 10 minutes at room temperature.
2. Measure absorbance at 540 nm in end-point mode at room temperature.

Note: Signal is stable for one hour after addition of Reaction Mix.

E. Live/Dead staining

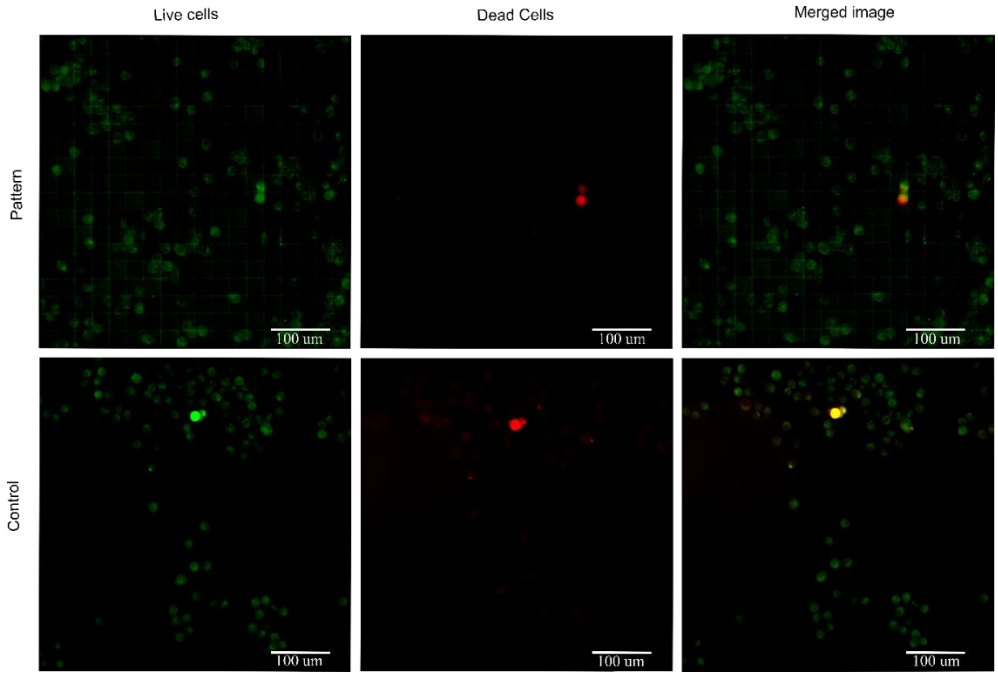

Figure 27: Live/Dead staining with cell density 50,000 cells/well

F. Geometrical characteristics of the patterns

Table 2: Geometrical characteristics of the patterns as designed and as measured. Measured values are given in average (standard deviation) format.

Pattern	$Pitch_d$ (nm)	$Pitch_r$ (nm)	Pillar $diameter_d$ (nm)	Pillar $diameter_r$ (nm)	Pillar $height_d$ (nm)	Pillar $height_r$ (nm)	Aspect $Ratio_d$ (-)	Aspect $Ratio_r$ (nm)
P1	700	710(0)	250	246(22)	300	333(19)	0.83	0.740(64)
P2	700	706(8)	250	266(22)	500	571(38)	0.50	0.456(31)
P3	700	704(7)	250	281(25)	1000	967(41)	0.25	0.291(23)
P4	1000	1014(8)	250	200(22)	300	410(57)	0.83	0.494(72)
P5	1000	1016(8)	250	260(30)	500	556(60)	0.50	0.471(61)
P6	1000	1013(11)	250	300(26)	1000	915(83)	0.25	0.330(34)

G. Coefficient of Variation (CV) calculation

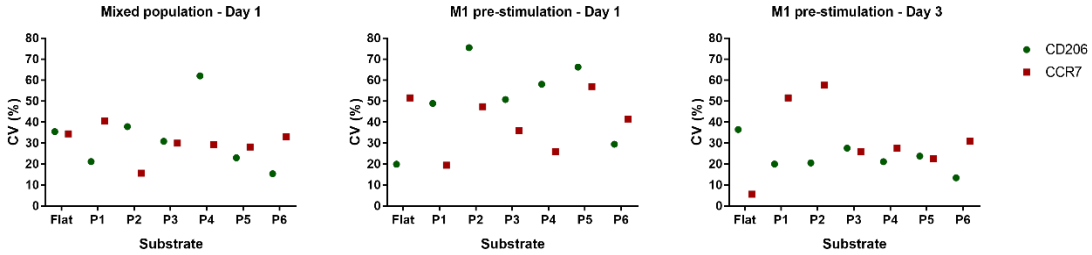

Figure 28: Coefficient of Variation (CV) in percentage (%) of the fluorescent intensity values per substrate per biomarker per experimental group.